



Water masses in the Atlantic Ocean: water mass ages and ventilation

Mian Liu^{1, 2} and Toste Tanhua²

¹School of Environmental Science and Engineering, Xiamen University of Technology, Xiamen, 361021, China

²GEOMAR Helmholtz Centre for Ocean Research Kiel, Marine Biogeochemistry, Chemical Oceanography, Wischhofstraße 1-3, 24148 Kiel, Germany

Correspondence to: Mian Liu (2023000069@xmut.edu.cn)

Abstract: The distribution of oceanic water masses and their properties, such as ventilation constitute fundamental parameters, for instance, the thermohaline circulation patterns and biogeochemical processes in the marine systems. The distributions of main water masses in the Atlantic Ocean have been comprehensively documented in a companion study (Liu and Tanhua, 2021), this study presents quantitative assessments of water mass age characteristics and ventilation time scales through multi-tracer analysis incorporating chlorofluorocarbon-12 (CFC-12), sulfur hexafluoride (SF₆), and argon-39 (³⁹Ar). Here we use two distinct age concepts: mean-age as an integrative metric of water mass chronology, and mode-age as a proxy for advective time scales. Empirical results demonstrate systematic age progression with increasing pressure and along water mass trajectories. Surface layer central waters exhibit mean ages up to ~100 years and mode ages reaching ~30 years. In the intermediate layer, meridional age gradients characterize the Antarctic Intermediate Water (AAIW) reaching maximum mean-age (~300 years) and mode-age (~80 years) at 30 °N, whereas zonal variations manifest in Mediterranean Water (MW) with peak values (~400 years in mean-age, ~100 years in mode-age) observed in equatorial regions. As the dominant deep water component, North Atlantic Deep Water (NADW) exhibits extreme ages in the Antarctic Circumpolar Current (ACC) region at 50°S, achieving mean age ~600 years and mode age ~100 years. Bottom layer water masses display their oldest signatures: Antarctic Bottom Water (AABW) from the Weddell Sea reaches ~600 years (mean) and ~100 years (mode) at equatorial latitudes, while its extension, Northeast Atlantic Bottom Water (NEABW), attains exceptional values of ~800 years (mean) and ~120 years (mode) at 50°N. The age analysis reveals significant basin-scale asymmetries, with eastern basins exhibiting younger ages compared to western counterparts. Ventilation efficiency modulates these age distributions, as evidenced by lower mode-ages and reduced apparent oxygen utilization (AOU) in better-ventilated western basins. The calculated oxygen utilization rate (OUR) demonstrates spatial concordance with dissolved oxygen (DO) concentrations, corroborating enhanced oxidative processes in high-oxygen regimes. This integrated age framework provides novel insights into water mass ventilation dynamics and their biogeochemical implications through quantitative characterization of temporal-spatial age distributions across multiple oceanographic provinces.

Key words: Water Mass, Atlantic Ocean, Transient Tracer, Mean- and Mode-age, Ventilation, GLODAPv2 data product



30 1 Introduction

31 The Atlantic Ocean is composed by a complex vertical stratification of water masses characterized by differences in properties
32 such as density. Liu and Tanhua (2021) have systematically characterized 16 main water masses that have been extensively
33 considered and studied due to their significant impacts on ocean circulation patterns and global climate regulation (e.g., Hall
34 & Bryden, 1982; Bryden et al., 2005; Kuhlbrodt et al., 2007; Clark et al., 2012). Ocean ventilation constitutes a fundamental
35 thermohaline process responsible for the vertical displacement of surface waters into the deep ocean, effectively redistributing
36 surface heat and salinity anomalies through density-driven stratification. This process inherently obeys the principle of mass
37 conservation, simultaneously enabling the upwelling of deep-sea waters to the surface ocean. The resultant vertical exchange
38 plays a critical role in maintaining global heat distribution patterns and sustaining the thermodynamic equilibrium of the ocean
39 system (Talley, 2013; Armour et al., 2016; Talley et al., 2016). Beyond its thermodynamic significance, ocean ventilation
40 emerges as a pivotal mechanism governing marine biogeochemical cycles. By mediating the downward transport of
41 atmospheric oxygen and carbon dioxide to abyssal depths, this process fundamentally regulates dissolved oxygen
42 concentrations and carbon sequestration rates in the deep ocean (Tanhua et al., 2006; Ziska et al., 2013; Skinner et al., 2017).
43 Related studies have further elucidated ventilation's deterministic role in controlling abyssal redox conditions and organic
44 carbon remineralization processes (van Heuven et al., 2011; Ito et al., 2016; Schmidtke et al., 2017).

45 Early studies of the water mass ventilation are proposed by Sandström already in the early 20th century (Sandström, 1908;
46 1916). Sverdrup and Bjerknes also reported the impacts of ventilation and currents on the climate through the air-sea
47 interactions (Sverdrup, 1940; Bjerknes, 1964). Hereafter many studies have been focusing on the ventilation. For instance,
48 Dickson et al., (1994) estimated the formation and pathway of the North Atlantic Deep Water (NADW) based on the
49 hydrodynamics, Orsi et al., (1999) investigated the circulation of the Antarctic Bottom Water (AABW) by using
50 Chlorofluorocarbons (CFCs). Recent studies suggest that the intensity of ocean ventilation varies with environmental factors,
51 such as intensity of the westerly winds (e.g. Rahmstorf, 2010; Purkey et al., 2010; Morrison et al., 2015). Several studies
52 investigate the regional scale or specific water masses, for instance, the upwelling of Circumpolar Deep Water (CDW) in the
53 Southern Ocean (Tamsitt et al., 2017), or the ventilation in the South China Sea (Wang et al., 2021). However, few studies
54 look at the ventilation over ocean basin scales, which is helpful to understand the effect of ocean-climate interactions, and in
55 addition can provide a basis for the biogeochemical studies.

56 The water mass age is an important parameter to evaluate the ventilation and refers to as the elapsed time on the pathway. The
57 CFCs and Sulfur hexafluoride (SF_6) are recognized as effective transient tracers for water masses and to estimate their ages
58 (Fine, 2011). The concentrations of CFCs in surface seawater increased continuously following the increase of the atmospheric
59 concentration since their introduction in the early 20th century (Gammon et al., 1982; Warner and Weiss, 1985). The use of
60 CFCs as a tracer in the oceanography is well established (e.g. Bullister and Weiss, 1983; Doney and Bullister, 1992; Fine,
61 2010; 2011), and transient tracers is a core variable in the GO-SHIP repeat hydrography program. Similarly, the transient tracer
62 is an Essential Ocean Variable (EOV) in the Global Ocean Observing System (GOOS) framework. SF_6 has been used as a new
63 tracer since mid-1990s complementing the CFCs due to the reduction of CFCs in the atmosphere (Maiss et al., 1996; Bullister
64 et al., 2002). The application of SF_6 is generally appropriate for recently formed water masses in the upper ocean (Tanhua et
65 al., 2008), i.e. for well ventilated, or young, waters. The CFCs are used to trace the relative deeper water masses (before mid-
66 1990s or partial pressure of CFC-12 lower than about 450 parts per trillion, ppt), while the SF_6 is the better choice for recently
67 formed shallow water masses (after mid-1990s or partial pressure of CFC-12 higher than about 450 ppt, Tanhua et al., 2008).
68 The complementary nature of CFCs and SF_6 allows for more accurate tracing of water masses (Law and Watson, 2001; Vollmer
69 and Weiss, 2002; Watanabe et al., 2003; Tanhua et al., 2004, 2005; Bullister et al., 2006). In addition, the application of
70 transient tracers also provides support to the hydrographic and biogeochemical field in calculating the upwelling velocity



71 (Tanhua and Liu, 2015) or estimating the ventilation and anthropogenic carbon cycle (van Heuven et al., 2011; Tanhua et al.,
72 2013; Patara et al., 2021).

73 As two typical representatives of transient tracers, the CFCs and SF₆ are commonly employed for determining water mass
74 ages, verifying hydrological models, and estimating rates of marine biogeochemical processes, such as anthropogenic carbon
75 storage and oxygen consumption. They exhibit advantages in tracing upper and middle water masses with relatively younger
76 ages. However, challenges arise when attempting to obtain data from deep and bottom layers with old waters. The chemically
77 inert isotope argon-39 (³⁹Ar), which has a half-life of 269 years, addresses this gap. ³⁹Ar is particularly advantageous for tracing
78 deep and bottom water masses with ages exceeding 500 years (Broecker & Peng, 2000; Holzer & Primeau, 2010; Lu et al.,
79 2014). Initially, its application was constrained by the requirement for large sampling volumes—typically around 1000 liters—
80 and the limitations of low-level counting (LLC) detection methods (Loosli et al., 1983; Schlosser et al., 1994; Schlitzer et al.,
81 1985). Consequently, ³⁹Ar was not widely utilized in oceanographic tracer studies. With advancements in Atom Trap Trace
82 Analysis (ATTA) technology (Chen et al., 1999; Jiang et al., 2011), ³⁹Ar has gradually gained prominence as an effective tracer
83 for investigating deep and bottom waters (Lu et al., 2014; Ebser et al., 2018), the accuracy and stability have also been
84 significantly improved (Jia et al., 2025). Therefore, the multi-parameter combination of CFCs, SF₆, and ³⁹Ar can transcend the
85 temporal limitations associated with single-tracer dating methodologies while providing more comprehensive insights into
86 biogeochemical processes. In this study, we introduce ³⁹Ar to investigate water mass ages within the Atlantic Ocean, in
87 particular for the older waters.

88 The apparent oxygen utilization (AOU, μmol kg⁻¹) is an important indicator in characterizing the respiration of organic matter
89 consuming oxygen, and balancing the oxygen supply through ventilation and photosynthesis. The oxygen utilization rate (OUR,
90 μmol kg⁻¹ yr⁻¹), which can be calculated from AOU and water mass age, is a significant parameter in estimating the
91 biogeochemical processes such as primary productivity or remineralization (e.g. Jenkins, 1982; Bender, 1990). The OUR has
92 been recognized to be a function of pressure for a long time (e.g. Tseitlin, 1992). However, the OUR is the integrated oxygen
93 consumption rate along the pathway of a water mass and represents a regional view of export flux (e.g. Stanley et al., 2012;
94 Koeve and Kähler, 2016), and thus an imperfect measure of local OUR. In this study, the OUR is calculated from water mass
95 ages estimated from the CFC-12 and SF₆. The change of OUR over time in different water masses are presented and the
96 impacts from the currents and topography are discussed.

97 In the study by Liu and Tanhua, (2021), the characteristics of main water masses in the Atlantic Ocean are defined by six key
98 properties, using the Global Ocean Data Analysis Project version 2 the annual update 2023 (GLODAPv2.2023, Lauvset et al.,
99 2016; Olsen et al., 2016; Lauvset et al., 2024) data product as a source of unbiased data. The static distribution of the water
100 masses is estimated with the Optimal Multi-Parameter analysis (OMP analysis, Karstensen and Tomczak, 1997; 1998). As a
101 continuation of that work, here we estimate the ventilation of water masses in the Atlantic Ocean with the combination of the
102 above mentioned three transient tracers (CFC-12, SF₆ and ³⁹Ar). The water mass ages are estimated and the OURs are
103 calculated. The goal of this study is to further improve the report of water masses in the Atlantic Ocean by adding the age as a
104 measure of ventilation, and to provide a hydrographic assistant for the biogeochemical researches.

105 2 Data and methods

106 2.1 Transient tracers and Inverse Gaussian Transit Time Distribution (IG-TTD)

107 Attempts have been made to find chemically stable tracers with large dynamic ranges in seawater as tracers that can be



reasonable easily measured. The prerequisite for transient tracers is 1) the concentration in the atmosphere increases (or decreases) monotonously in the history; 2) their surface concentration is equilibrium to the atmosphere, or the saturation state over time can be estimated; 3) their input functions are known; 4) there are no sources or sinks in the ocean interior. The solubility (F) of gaseous transient tracers in the seawater is a function of potential temperature (θ) and practice salinity (S) (e.g. Warner and Weiss, 1985; Bullister et al., 2002).

By considering the diffusive ocean where mixing is important, Waugh et al., (2003) applied the concept of transit time distribution (TTD, Hall and Plumb, 1994) to the ocean interior:

Tracer-age ($c(t)$) is the time that water mass takes from surface to the deeper layer.

$$c(t) = c_0(t - \tau);$$

Mean-age (Γ) shows the average of ages in different parts of a water sample from different pathways.

$$\Gamma = \int_0^\infty \xi G(\xi) d\xi;$$

Width (Δ^2) describes the mixing and the diffusion in the ocean.

$$\Delta^2 = \frac{1}{2} \int_0^\infty (\xi - \Gamma)^2 G(\xi) d\xi;$$

The relationship between all the above parameters is often assumed to follow the inverse Gaussian function.

$$G(t) = \sqrt{\frac{\Gamma^3}{4\pi\Delta^2 t^3}} \exp\left(\frac{-\Gamma(t-\Gamma)^2}{4\Delta^2 t}\right);$$

In these equations t , Γ and Δ describe the tracer-age, mean-age and the width of TTD. In the ocean reality, the mixing ratio (Δ/Γ) indicates the situation of advective (low ratio) or diffusive (high ratio) dominated mode of water transport. Although it is possible and conceivable that other solutions to the TTD than an Inverse Gaussian (IG) function best describes the ventilation age of a water mass, we apply the IG solution to the TTD in this work. For instance, Stöven and Tanhua, (2014) concludes that a 2-IG distribution is necessary to explain ventilation ages in the Mediterranean Sea. The TTD concept also assumes a steady state ocean, circulation, a condition that is often not fulfilled. For this application however we use the 1-IG concept since solving other possibilities is not possible with the few collocated transient tracer observations available. Based on the TTD determined from the tracer observations, Wang et al., (2021) estimated the OUR in the northern South China Sea.

2.2 Definitions in the age of a water mass: tracer-age, mean-age and mode-age

The concept of a water mass age is defined as the time elapsed from that a water mass was in contact with the atmosphere at the surface in the formation area (Thiele and Sarmiento, 1990). The concentrations of transient tracers (CFC-12 and SF₆ in units of mol kg⁻¹) can be observed directly in the interior ocean and the partial pressures can be calculated combining with the potential temperature (θ in °C) and practical salinity (S). With the TTD concept, three different flavors of water mass ages are often used as derived from observations of transient tracers; the tracer-age, the mean-age and the mode-age.

The tracer-age shows the elapsed time from the surface of the formation area to the interior ocean at the sampling location (Fig. 1, a) by simply matching the observed tracer fields with the atmospheric history of the tracers. In other words, the tracer-



age assumes the ocean is purely advective, without diffusion. This definition is simple to apply as a TTD do not need to be considered, i.e. the TTD is only one spike. However, the diffusion cannot be neglected in the realistic oceans, so the actual ages of water masses are underestimated by the tracer-age. The concept of TTD is applied in order to correct such underestimation. A definition of mixing ratio (Δ/Γ , see below) is defined as the width of an Inverse Gaussian (IG) distribution over the ages to indicate the advective (low ratio) or diffusive (high ratio) situation. From the IG distribution, the mean-age and mode-ages can be calculated. The mean-age is obtained by the average value of all the different aliquots in one water sample by considering the transport time of different pathways (Fig. 1, b). This concept of water mass age is often useful for biogeochemical studies. In other cases, such as when discussing the transport times of water masses from the formation area, the mode-age concept is useful. From the physical perspective, the mode-age reflects the age of the dominate water mass in the sample, i.e. the mode-age shows the time (t) when the Inverse Gaussian Distribution ($G(t)$) reaches the maximum (Fig. 1, b).

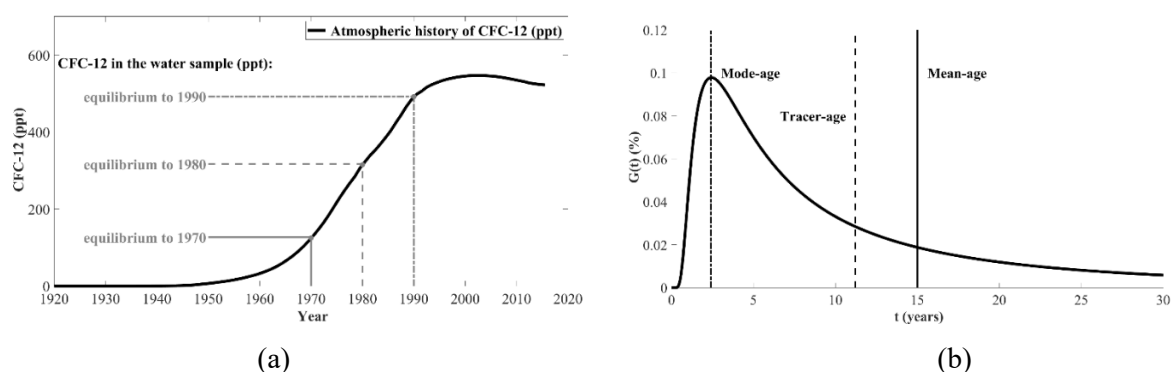


Figure 1. Concepts of three flavors of water mass ages.

(a) The tracer-age shows the transient tracers in the water samples are equilibrium to which year of the atmospheric history and assumes the ocean as purely advective; (b) The concept of tracer-age, mean-age and mode-age are shown in the IG-TTD assuming that CFC-12 = 300 ppt and $\Delta/\Gamma = 1$ for a sample from 1990.

2.3 Determination of the mixing ratio (Δ/Γ):

The atmospheric concentration increased monotonically until mid-1990s for the CFC-12 and is still increasing for the SF₆ (Fig. 2, a). In addition, the mixing ratio (Δ/Γ) also plays a significant role in the calculation of mean-age and mode-age. Under the assumption for a particular tracer concentration, for instance 300 ppt for the CFC-12 in the sampling year 1990, the mean-age increases with the mixing ratio (Δ/Γ), since the “tail” of the Inverse Gaussian Function becomes longer, while the mode-age decreases with the mixing ratio (Δ/Γ) as the “peak” appears earlier (Fig. 2, b).

The significance of mixing ratio to the age calculations is also evident in the observations. The cruise along the A16 section in 2013 (Fig. 3, a) shows that different ratios lead to significant differences in water mass ages, especially when the partial pressures of tracers are low (CFC-12 lower than 50 ppt and SF₆ lower than 0.2 ppt) (Fig. 3, b and c). The mean-ages show relative low values when the ocean is assumed to be a relatively advective ($\Delta/\Gamma < 0.8$). Most mean-ages below 1500 dbar are between ~300 and 700 years, with some mean-ages around 20 °N even higher than ~700 years (although this is close to the detection limit for the corresponding CFC-12 concentrations). In contrast, the mean-ages are generally higher than ~700 years with diffusive ($\Delta/\Gamma > 1.4$) assumption (Fig. 3, b). The situation of mode-ages is the opposite. The mode-ages are higher, mostly between ~50 and 100 years in the intermediate layer, higher than ~100 years in the deep and bottom layer and above



~150 years around 20 °N under the advective ($\Delta/\Gamma = 0.8$) assumption, while most mode-ages show low values around ~50 years under the diffusive ($\Delta/\Gamma = 1.4$) assumption (Fig. 3, c).

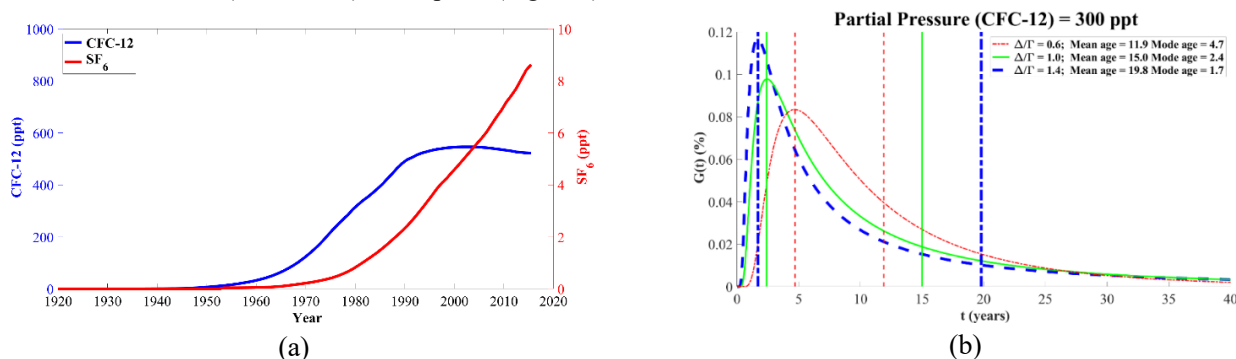


Figure 2. The relationships between mean-age, mode-age and mixing ratio (Δ/Γ).

(a) Atmospheric historical partial pressure of transient tracers over time (CFC-12 and SF₆) in the North Hemisphere;
(b) Relationship between mean-ages and mode-ages under same partial pressure (CFC-12 = 300 ppt) but different mixing ratios (Δ/Γ) in the sampling year 1990.

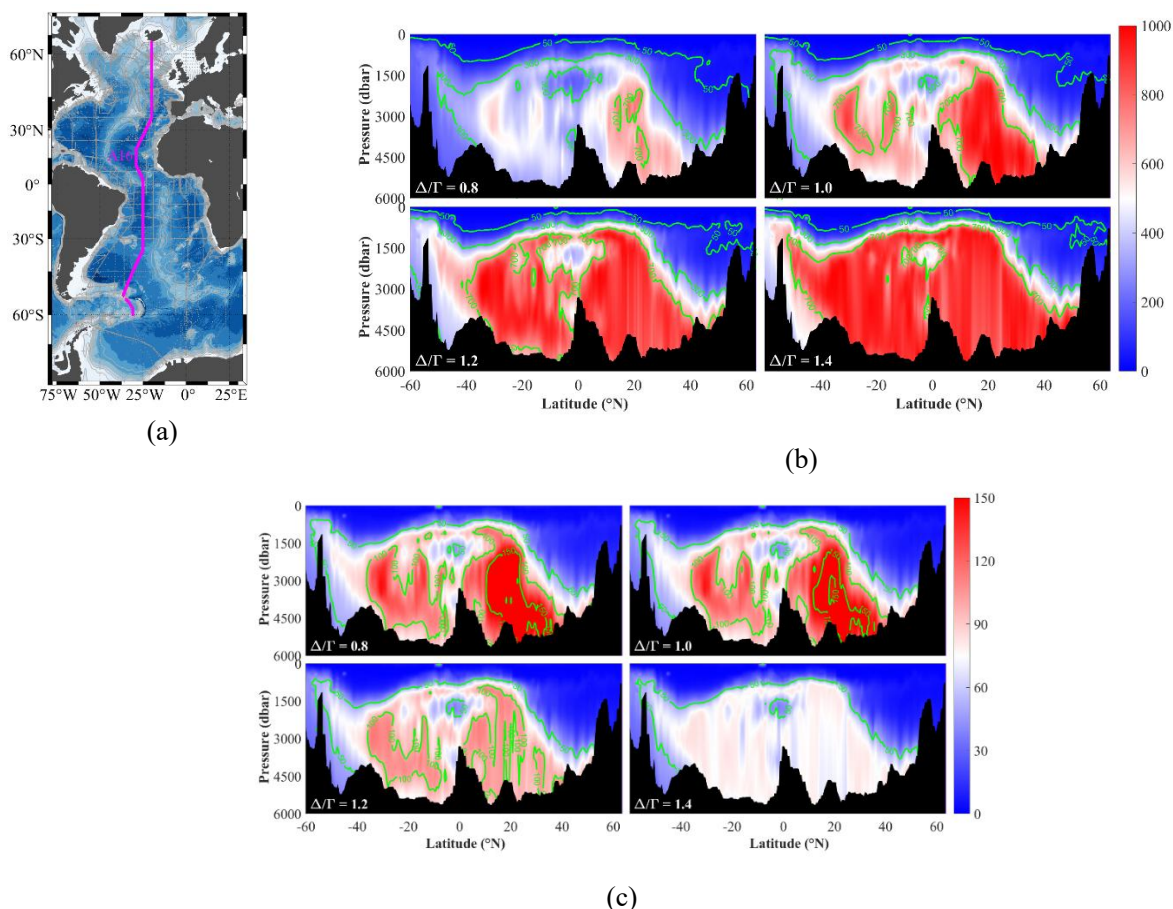


Figure 3. The A16 section of WOCE/GO-SHIP in 2013 (a) and the distributions of mean-ages (b) and mode-ages (c) with different mixing ratios ($\Delta/\Gamma = 0.8, 1.0, 1.2, 1.4$) based on the GLODAPv2 observational data



The determination of the shape of the TTD, i.e. of the mixing ratio (Δ/Γ) if you assume an Inverse Gaussian distribution, is one of the prerequisites before estimating the ages of water masses. In the specific regions with a small-scale calculation, or under a typical diffusive or convective situation where the mixing ratio is quite different from 1, a corresponding value of mixing ratio (Δ/Γ) according to the specific situation is required to obtain the relative accurate water ages (Vaugh et al., 2004; Schneider et al., 2014). However, in most cases the lack of independent tracer data limits the options to empirically estimate mixing ratios in most areas. In order to calculate the distribution of transient tracers and the ages of water masses over the Atlantic Ocean, a reasonable assumption is the standard mixing ratio ($\Delta/\Gamma = 1$, Vaugh et al., 2004; Stanley et al., 2012; Thomas et al., 2020) for the general calculations (Schneider et al., 2010; Huhn et al., 2013; Stöven and Tanhua, 2014). In this study, the standard mixing ratio ($\Delta/\Gamma = 1$) is followed to estimate the mean-ages and mode-ages of water masses in the Atlantic Ocean.

3 Results: Ages of water masses in the Atlantic Ocean

In this study, we follow the division of vertical layers and distributions of water masses presented by Liu and Tanhua (2021), but now focus on the transient tracers and water mass ages. Three hydrographic sections are selected from the WOCE/GO-SHIP sections in this work to represent the mean-ages of the main water masses (Table 1). The A16 sections in 2013 (Expo-code 33RO20130803 and 33RO20131223) show the meridional distribution across the whole Atlantic Ocean, while the A05 section in 2010 (Expo-code 74DI20100106) and A10 section in 2011 (Expo-code 33RO20110926) show the zonal distributions in the North and South Atlantic Ocean respectively (Fig. 4). The partial pressures of CFC-12 and SF₆ along the above sections are shown in Fig. 4 (Only CFC-12 data are displayed along A05 section due to the lack of SF₆ data in this section). Both tracers show similar distributions with high values in the shallow layers, and a general decrease with increasing pressure.

Table 1: Expo-code, Ship, Chief scientists and PI of transient tracers for the selected hydrographic cruises to the Atlantic Ocean showed as sections in this study

WOCE/GO-SHIP section	Year	Expo-code	Ship	Chief Scientist	PI of transient tracers
A16N	2013	33RO20130803	Ronald H. Brown	John Bullister & Molly Baringer	John Bullister
A16S	2013	33RO20131223	Ronald H. Brown	Rik Wanninkhof	John Bullister
A05	2010	74DI20100106	Discovery	Brian King	Marie-José Messias
A10	2011	33RO20110926	Ronald H. Brown	Molly Baringer	John Bullister

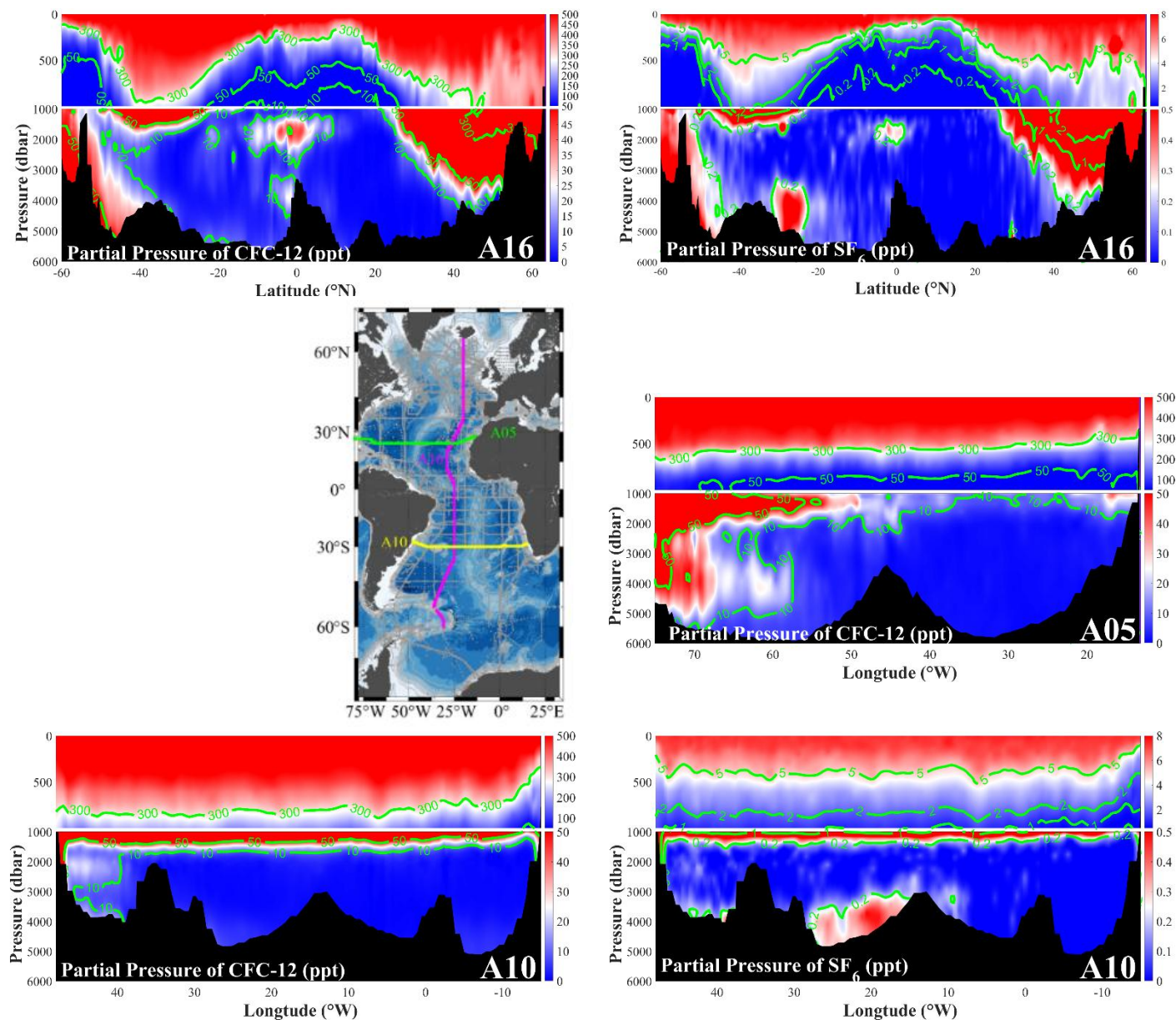


Figure 4. Map of three selected WOCE/GO-SHIP sections to represent the ages of the main water masses in the Atlantic Ocean (middle left) and partial pressures of CFC-12 and SF₆ along the three selected sections. Note the different colorbars between upper and lower parts divided at pressure of 1000 dbar.

188 In this study, CFC-12 is used to estimate water mass ages when the partial pressures of CFC-12 are lower than 450 ppt, while
 189 the SF₆ is used when the partial pressures of CFC-12 are higher than 450 ppt according to Tanhua et al., (2008). The
 190 distributions of partial pressures mean that the upper layer have the lowest mean-ages within ~100 years and mode-ages within
 191 ~30 years (Fig. 5). The distributions of mean-ages and mode-ages also show spatial differences in the horizontal direction.
 192 Relatively low ages are found in the high latitude regions (Fig. 5, a and b). This indicates that the deep water masses are newly



193 formed here, and thus have low ages. In the region between 20 and 40 °N, the mean-age reaches the peak value up to ~1000
194 years and the mode-age up to ~150 years, suggesting the sluggish water exchange and long residence time of old water masses.
195 In the zonal direction, both mean-ages and mode-ages are significantly lower in the west in the general region below 1500m
196 dbar, suggesting that these regions are better ventilated due to the western boundary current (Fig. 5 c to f).

197 In the analysis of water mass ages in each layer, maps with mean-ages and mode-ages in each station are firstly presented as a
198 qualitative overview. The mean values of the ages at the core pressure of each water mass are plotted at certain station. In
199 addition, the quantitative calculations are made along the three selected sections to represent the distributions of water mass
200 ages in detail and estimate the impacts from currents and mixing.

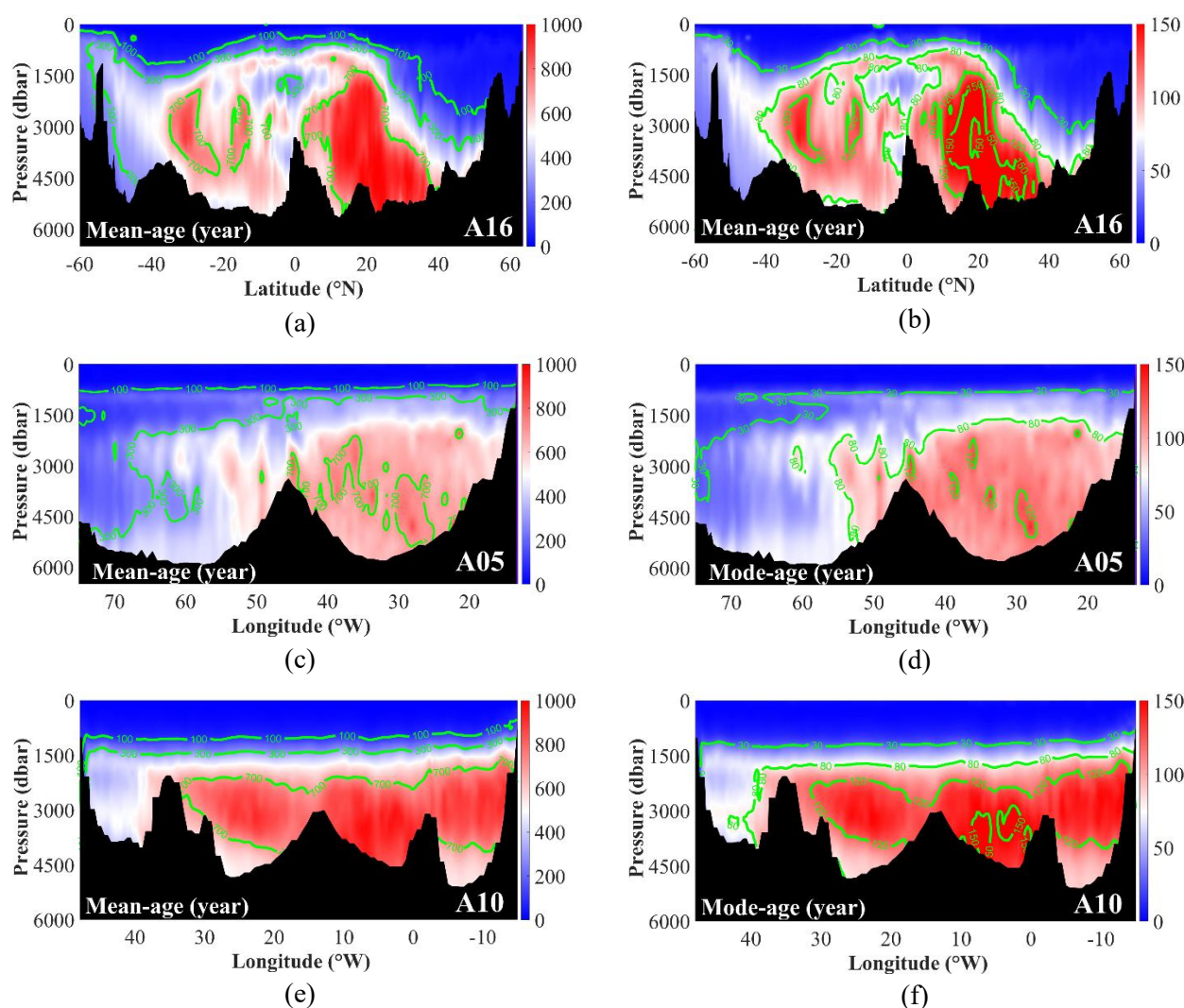


Figure 5. Mean-ages and Mode-ages along the three selected WOCE/GO-SHIP sections



202 3.1 The upper layer

203 The spreading of central waters can be traced by the distributions of ages. After leaving their formation areas in the mid-
204 latitude regions, the West North Atlantic Central Water (WNACW) and West South Atlantic Central Water (WSACW) spread
205 generally in zonal direction towards the formation areas of the East North Atlantic Central Water (ENACW) and East South
206 Atlantic Central Water (ESACW) with Azores Current and South Atlantic Current, respectively (Fig. 6, a). The mean-ages
207 show that the “mixed” age of all the compositions in the western central waters is ~50 years (Fig. 6, b and Fig. 7). When
208 focusing on the main body of WNACW and WSACW, the mode-ages show that the advective time-scale is ~15 years for both
209 water masses (i.e. Both WNACW and WSACW take ~15 years from the formation area to the equator, Fig. 6, c and Fig. 7).
210 At greater depths, the ENACW and ESACW are transported from their formation areas and spread with the main currents
211 towards the equator (Fig. 6, a). In the northern hemisphere, the ENACW spreads southward with the Canary Current, while
212 the ESACW in the southern hemisphere is transported northward with the Benguela Current and the South Equatorial Current.
213 The difference in mean-age is ~100 years between the formation areas and the equatorial region (Fig. 6, b and Fig. 7). The
214 mode-ages indicate that the main body of ENACW and ESACW takes approximately 30 years to be transported from formation
215 areas to the equator (Fig. 6, c and Fig. 7). The central waters occupy the upper layer above the neutral density isoline of 27.10
216 kg m^{-3} . The core pressures of western and eastern central waters are around the neutral density (γ) of 26.5 and 26.9 kg m^{-3}
217 respectively (Liu and Tanhua, 2021). The ages of central waters at their core neutral densities are shown in Fig. 6. The eastern
218 central waters have mean-ages of up to approximately 100 years and mode-ages up to approximately 30 years, while the
219 western central waters are younger with ages of ~50 years and ~15 years respectively (Fig. 6). The relatively low ages in the
220 upper layer indicate that these water masses are newly formed. In the meridional direction along the A16 section, both mean-
221 ages and mode-ages show low values of around 20 years in the mid-latitude regions that are close to the formation areas of
222 central waters (Fig. 6 and Fig. 7). In contrast, the ages are higher (~100 years for mean-age and ~30 years for mode-ages) in
223 the tropical region. In the zonal direction, the ages in the eastern basin are slightly higher than in the western basin for the
224 central waters, but the difference is only within ~10 years for both mean-ages and mode-ages, indicating that the influence
225 from western boundary current is not significant in the upper layer. (Fig 7).

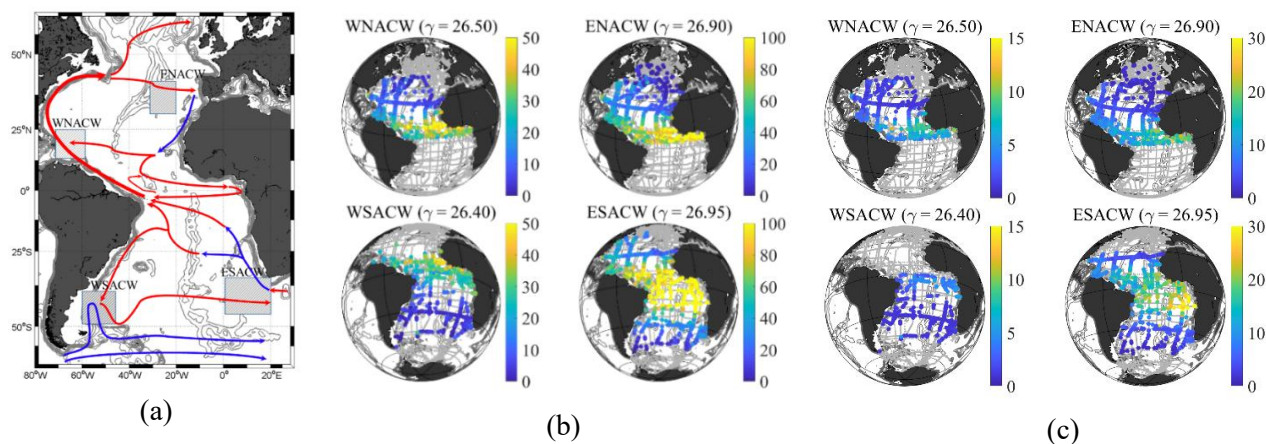


Figure 6. Ages of central water masses in the Atlantic Ocean.

(a) The main currents in the upper layer with warm (red) and cold (blue) currents and the approximate formation areas (rectangular shadows) of central water masses.

(b) The mean- and (c) mode-ages of central water masses at their core neutral densities (kg m^{-3}). The colored dots show the ages in each station. The grey dots show all the GLODAPv2 stations that have less than 20% contribution of the water mass in question or lack of transient-tracer data.

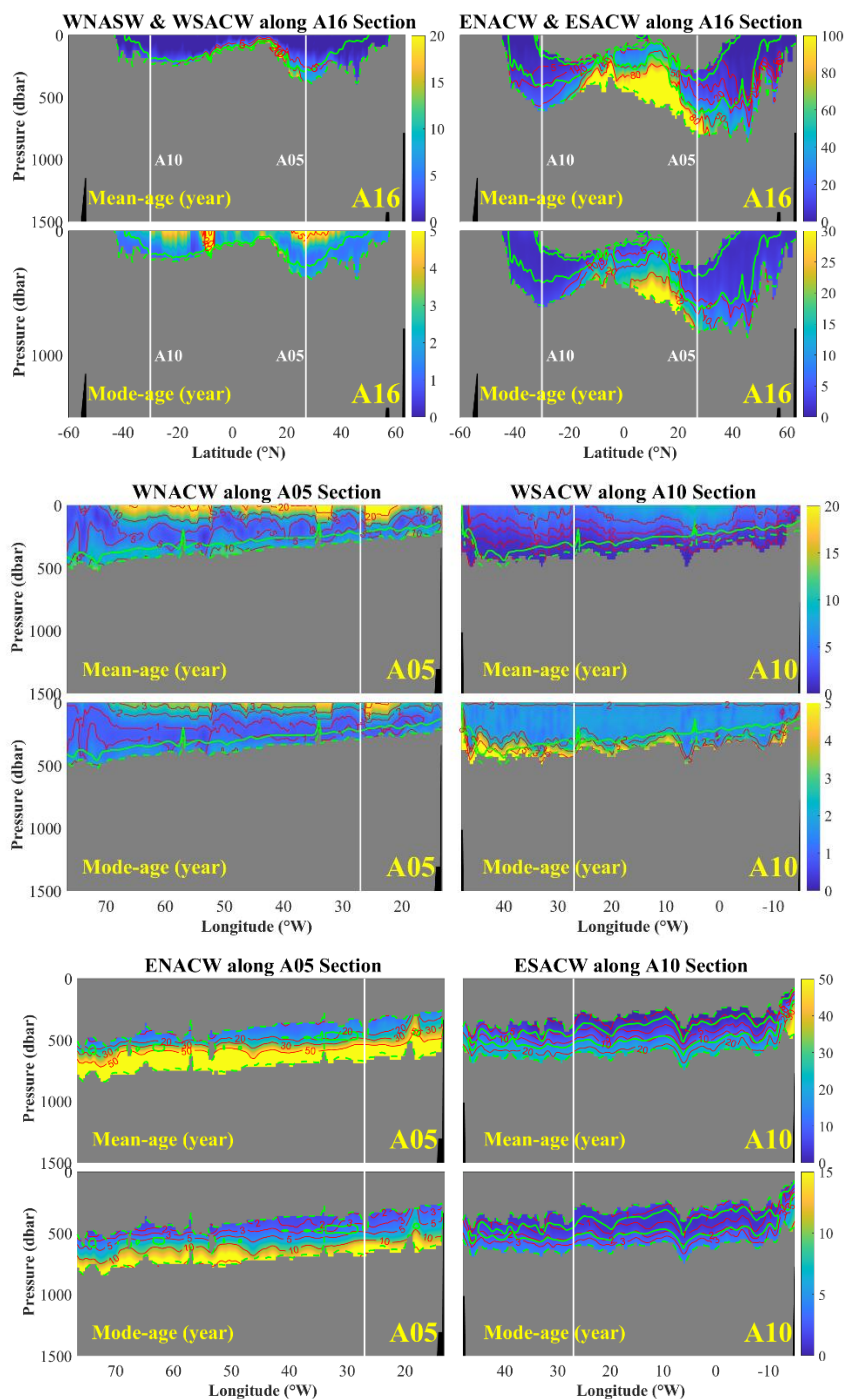


Figure 7. The mean- and mode-ages of central waters along the three sections for the upper 1500 dbar. The solid green isolines show the 50% fractions of water masses and the dashed green lines show the 20 % fractions. The grey color indicate areas with less than 20% contribution from central waters. White vertical lines show cross overs with other sections.



3.2 The Intermediate Layer

Three main water masses belong to the intermediate layer (γ between 27.10 and 27.90 kg m⁻³), including the Antarctic Intermediate Water (AAIW), the Subarctic Intermediate Water (SAIW) and the Mediterranean Water (MW). The ages of SAIW are not displayed in this study due to the lack of tracer data with a complete section through in the distribution region of this water mass.

Antarctic Intermediate Water (AAIW): The AAIW spreads from the formation area between 40 and 50 °S northward to approximately 30 °N along the Western Boundary Current (WBC) (Fig. 8, a). The northward flow of this water mass is part of the Atlantic western boundary current system (Talley, 1996) and the upper limb of AMOC (Kirchner et al., 2009).

Compared to the central waters, AAIW has significantly higher ages. In principle, the AAIW is supposed to get higher ages towards the north. In the meridional direction, the mean- and mode-ages increase from 0 to ~300 years and ~80 years from formation area to the equator, and further increase up to ~400 years and ~100 years respectively to 20 °N (Fig. 8 and 9). However, both ages decrease instead and approach even towards 0 in the further north region between 20 °N and 30 °N (Fig. 8, b and c), giving the impression of the AAIW being younger in the north Atlantic Ocean. The reason for the above result is the intervention from surrounding water masses. The maximum distance of AAIW to the north can reach 30 °N, but between 20 °N and 30 °N, this water mass mixes with the ENACW and upper NADW (Fig. 7, a, Fig. 9, a and Fig. 11, a), which origins from the Labrador Sea Water (LSW, Liu and Tanhua, 2021). Both ENACW and upper NADW are newly formed in this region, so the “mixed” AAIW obtains younger ages. Age differences are also found in the zonal direction. In better ventilated western basins, the AAIW transports northward with the western boundary current (WBC), so the mean- and mode-ages are lower. By contrast, the ages are significantly higher in the eastern basins with poor ventilation. The mean-ages reach ~400 years and the mode-ages are up to ~100 years in the east between 0 and 20 °S (Fig. 8, b and c). The mean- and mode-ages along the A05 section also show the zonal difference (Fig. 9, b). In the eastern basin (east of the Mid-Atlantic-Ridge, MAR), the mean-age and mode-age appears up to ~400 and ~80 years respectively, in contrast only ~200 years and ~50 years in the west. This distribution confirms that the AAIW is transported by the WBC and takes a longer time to cross the MAR. Generally lower ages are found along the A10 Section in contrast to the A05 Section due to closer distance to the formation area of AAIW (Fig. 9, c). Similar zonal difference exists with mean-ages of ~50 years in the west ~100 years in the east and mode-age of ~10 years in the west and ~20 years in the east.

Both mean- and mode-ages of AAIW also show differences in the vertical direction due to the mixing with other water masses. At the shallow boundary to the upper layer, the AAIW mixes with “younger” eastern central waters. At the lower boundary to the deep and overflow layer, the northward flowing AAIW mixes with the southward flowing upper NADW. Along the A10 section, the upper NADW has experienced long spreading times and obtained a high mean-age of ~600 years and a mode-age of ~80 years (Fig. 11). As a result, the “mixed” ages between AAIW and upper NADW (~300 years for mean-age and ~60 years for mode-age) are relatively high at the border compared to the ages at core of AAIW (~100 years for mean-age and ~20 years for mode-age, Fig. 9, c). The situation is the opposite along the A05 section: The AAIW is old in the north Atlantic, while the upper NADW here is still relatively young. The “mixed” mean-age is ~200 years and mode-age is ~50 years in contrast to ~300 years for the mean-age and ~60 years for mode-age at the core of AAIW (Fig. 9, b). This result is consistent with the ages of NADW in the next section.

Mediterranean Water (MW): The MW is referred to as the product of the Mediterranean Overflow Water (MOW) that flows across the Strait of Gibraltar and mixes with the ENACW (Liu and Tanhua, 2021). This water mass is formed in the Gulf of



265 Cadiz where the MOW exits the Strait of Gibraltar as a deep current and turns into two branches (Fig 8, a). The northward
266 branch spreads into the West European Basin until 50 °N, while the westward branch spreads across the MAR into the west
267 basin of the North Atlantic Ocean (Price et al., 1993; Carracedo et al., 2016).

268 The spreading of MW can also be traced by the transient tracers (Fig 9, a), in addition to the water mass variables that goes
269 into the OMP analysis (Liu and Tanhua, 2021). The ages of MW have an increasing trend towards the south (Fig. 8, b and c).
270 The northward flow spreads faster so the mean-age is ~100 years and the mode-age is ~20 years at 50 °N. In contrast, the
271 southward flow shows a higher mean-age of ~400 years and mode-age of ~100 years at 25 °N along the A05 Section (Fig 9,
272 b). In the zonal direction, the ages decrease to the west (Fig 9, b), since the fraction of MW is only between 20% and 30%
273 along this section (green dash contour lines in Fig 9, b), and is therefore influenced by the lower ages from the NADW.

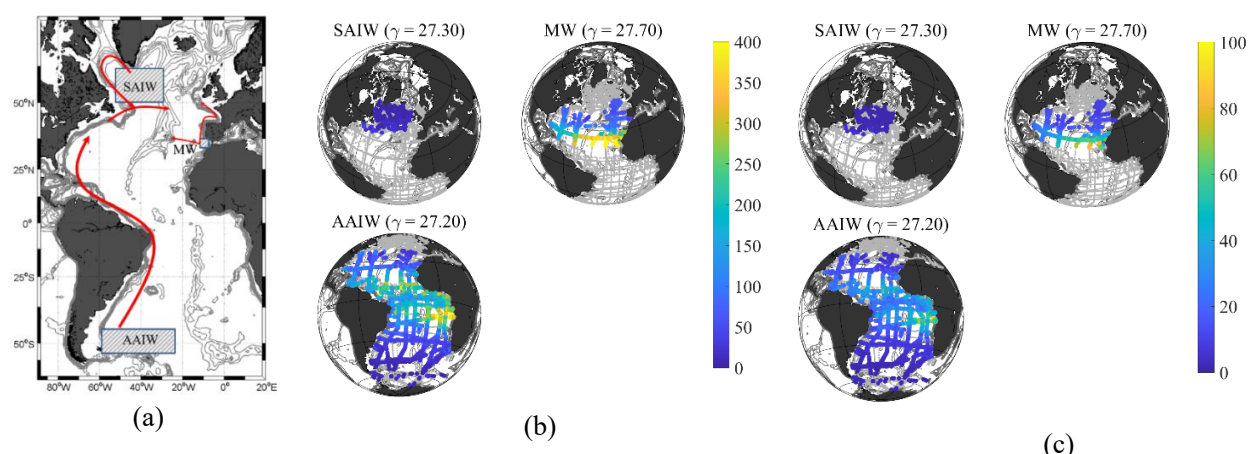


Figure 8. Ages of intermediate water masses in the Atlantic Ocean.

(a) Main currents in the intermediate layer. The currents (arrows) and the formation areas (rectangular shadows) of water masses in the intermediate layer.

(b) The mean- and (c) mode-ages of intermediate water masses at their core neutral densities (kg m^{-3}). The colored dots show the ages in each station. The grey dots show all the GLODAPv2 stations that have less than 20% contribution of the water mass in question or lack of transient-tracer data.

274

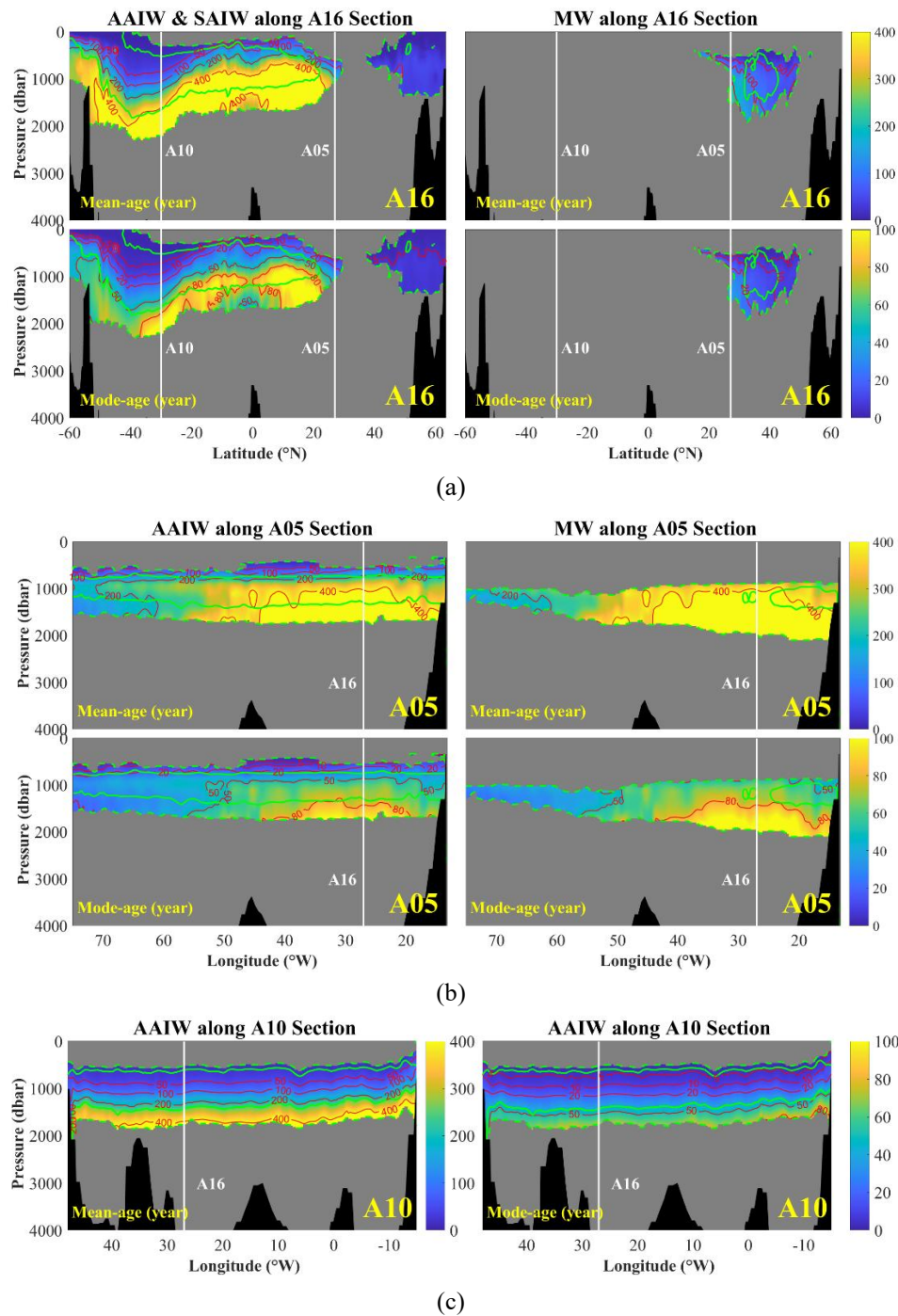


Figure 9. Mean- and mode-ages of intermediate water masses along the three sections for the upper 4000 dbar. The solid green isolines show the 50% fractions of water masses and the dashed green lines show the 20 % fractions. The grey blank indicates less than 20% contribution from intermediate water mass. White vertical lines show cross overs with other sections.



3.3 Deep and Overflow Layer

The North Atlantic Deep Water (NADW), including its upper and lower portions, dominates the deep and overflow layer (γ between 27.90 and 28.10 kg m^{-3}) of the Atlantic Ocean. This water mass is formed in the high latitude region in the North Atlantic and spreads southward at pressures between 2000 and 4000 dbar until it meets AAIW and AABW in the Antarctic Circum-polar Current (ACC) region. The southward spreading pathway is along the Deep Western Boundary Current (DWBC, Fig. 10, a). Meanwhile, the NADW also extends eastward with the eddies and finally covers the deep and overflow layer (Dickson and Brown, 1994).

Upper and lower North Atlantic Deep Water (NADW): The NADW is a water mass that is transported far southward from its formation area, with a mean-age of ~ 600 years (Fig. 10, b) and mode-age of ~ 100 years (Fig. 10, c) at the southern limb in the Antarctic Circum-polar Current (ACC) region. The increasing ages during the pathway to the south is shown along the A16 section (Fig. 11, a). After leaving the formation area, the mean- and mode-ages increase ~ 200 and ~ 20 years respectively from 60°N to 40°N . Afterwards, a sharply increase in both ages appear in the region between 30°N and 10°N . In this interval, the highest value of mean-age reaches ~ 1000 years and the mode-age is up to ~ 150 years. This is because the A16 section at this latitude range passed through the east part of the Atlantic Ocean (east of MAR) and the distance from the Deep Western Boundary Current (DWBC, Fig. 4 and Fig. 10, a) was high. High ages in this region are due to the sluggish water exchange over ridge. This result can also be confirmed by the observation along the A05 Section (Fig. 11, b): The NADW near the DWBC region has a low mean-age of ~ 200 years and mode-age of ~ 40 years, while the ages are up to ~ 600 years and ~ 100 years east of the MAR. After passing the equator, when the A16 section returns to the west of the MAR, the mean-ages of NADW are ~ 400 years and the mode-ages are ~ 80 years in the latitude range between 0 and 20°S , which further increase to ~ 600 (mean-ages) and ~ 100 (mode-ages) years along the pathway southward until 40°S . In the ACC region between 40°S and 60°S , the mean- and mode-ages of upper and lower NADW decrease to ~ 400 and ~ 80 years respectively. Similar to the situation of AAIW in the north Atlantic, this is also the result of mixing with newly formed AAIW and AABW. The spreading of NADW in the zonal direction is slower eastward, so the ages are generally higher in the eastern basin of the Atlantic Ocean (Fig. 10, b and c). The tracer data along the A05 and A10 sections also reflect the above result. In the A05 section, the mean-ages are ~ 200 years in the west and ~ 600 or even ~ 800 years in the east, and the mode-ages show ~ 50 years in the west and ~ 100 to ~ 120 years in the east (Fig. 11, b). In the A10 section, the mean-ages are ~ 400 years in the west and ~ 800 years in the east and the mode-ages are ~ 80 years in the west and ~ 120 years in the east (Fig. 11, c).

In the vertical direction, the upper NADW mixes with the AAIW from above and the lower NADW mixes with the AABW from below. As the NADW is transported in the opposite direction to these two water masses, the “mixed” ages in the north, which is closer to the formation area of NADW, are higher than the age at the core density of NADW, while the opposite situation exists when spreading to south. After entering the ACC region, both mean-age and mode-age even decrease since the fractions of newly formed AAIW and AABW are high.

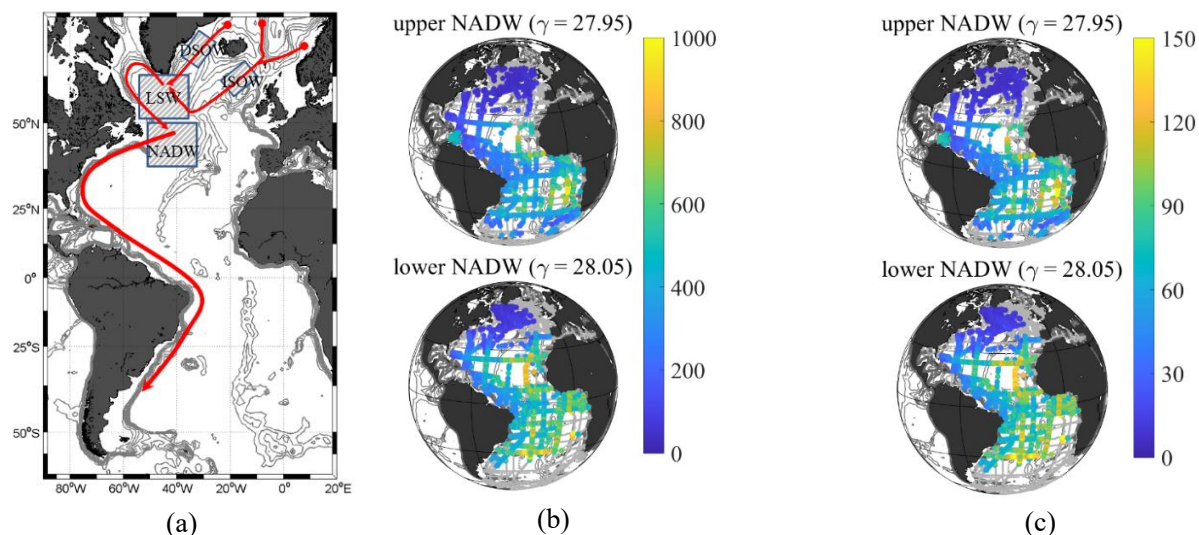


Figure 10. Ages of upper and lower NADW in the Atlantic Ocean.

- (a) Main currents in the deep and overflow layer. The currents (arrows) and the formation areas (rectangular shadows) of water masses in the deep and overflow layer.
- (b) The mean- and (c) mode-ages of upper and lower NADW at their core neutral densities (kg m^{-3}). The colored dots show the ages in each station. The grey dots show all the GLODAPv2 stations that have less than 20% contribution of the water mass in question or lack of transient-tracer data.

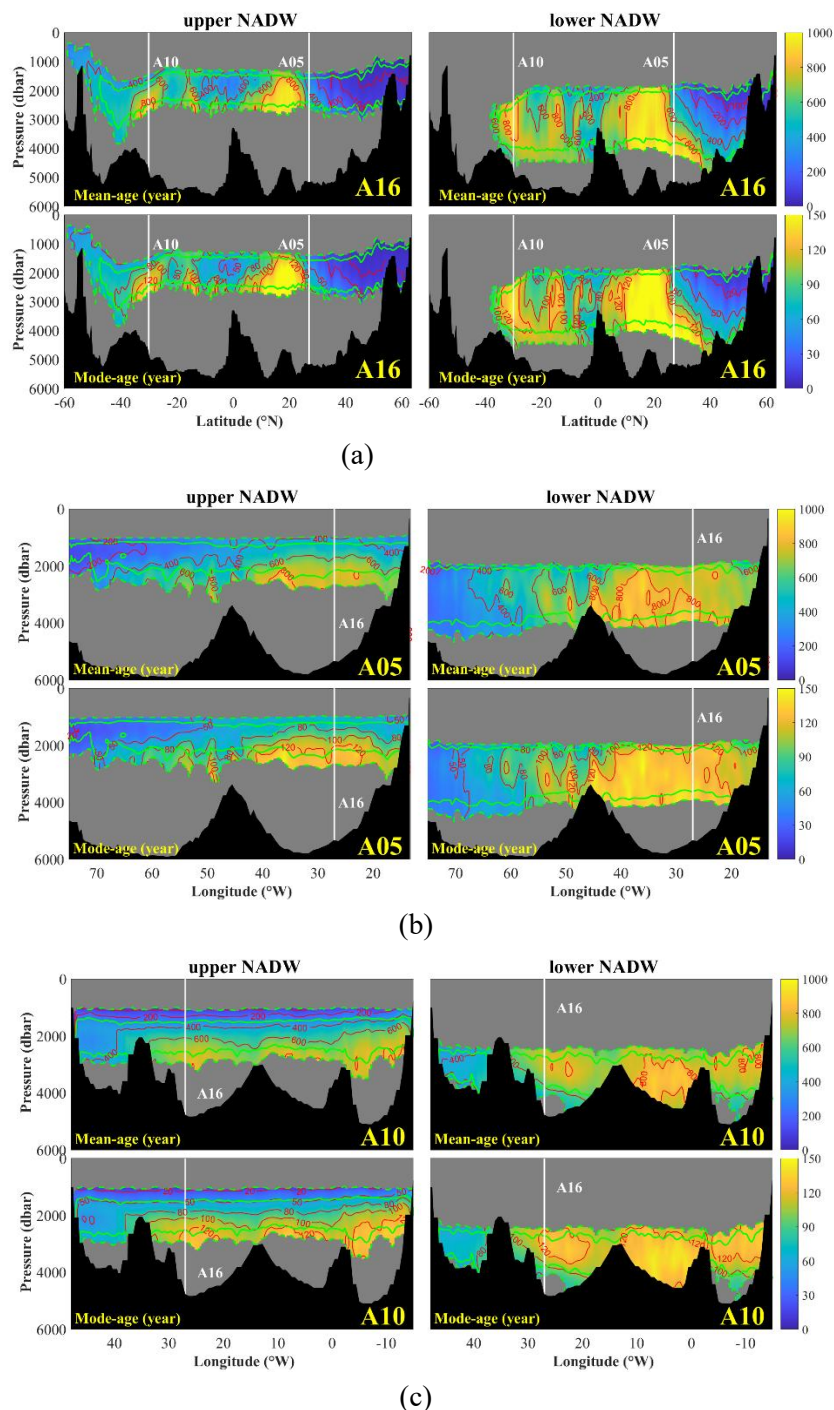


Figure 11. Mean- and mode ages of upper and lower NADW along the A16 (a), A05 (b) and A10 (c) section lines. The green contour lines show fractions of water masses in 50 % and the dashed green lines show the 20 % fractions. The grey blank indicates less than 20% contribution from NADW. The white vertical lines show cross overs with other section lines.



3.4 Bottom Layer

The bottom layer is noticed already by Wüst, (1933) as it is filled with water from the south. Sverdrup, (1940) further pointed out the role of ACC plays in the formation and spreading of Antarctic Bottom Water (AABW). On this basis, Mantyla and Reid, (1983) elaborated that the most original dense bottom water is restricted near the Antarctic region by topography and the northward flow of bottom water is the mixture of original dense water and the overlying warm water. Gordon and Huber (1990) and Orsi et al., (1999) illustrated that the pathway of AABW to the north is through the Drake Passage sill into the Argentina and Brazilian Basin (Fig. 12, a). In the Atlantic Ocean, the AABW dominates the bottom layer ($\gamma > 28.10 \text{ kg m}^{-3}$), which originates from the Weddell Sea and spreads to the north. After passing the equator, the AABW is redefined as Northeast Atlantic Bottom Water (NEABW, Liu and Tanhua, 2021).

Antarctic Bottom Water (AABW) & Northeast Atlantic Bottom Water (NEABW): The transport of bottom water is a long process going from the south towards the north. In the meridional direction, the AABW is transported towards the equator with a mean-age of ~600 years and mode-age of ~100 years at the equator, and further northward as NEABW to 40 °N with a mean-age of ~1000 years and mode-age of ~150 years (Fig. 12, b and c). Combined with the A16 Section, more specific segments/details can be seen. In the early stage from the surface of Weddell Sea to the bottom (below the pressure 4000 dbar) at 40 °S, the mean-age of AABW is ~300 years and mode-age is ~50 years. In the range between 10 and 30 °S, high values of ~800 years (mean-age) and ~120 years (mode-age) appear due to the mixing with the lower NADW with high ages (Fig. 13, a). After passing the equator, the redefined NEABW contains a mean-age up to ~1000 years and mode-age up to ~150 years at 40 °N, indicating that the bottom water, including the AABW and NEABW, takes about 150 years (mode-age) for the transport from the formation area (Weddell Sea) to 40 °N. North of 40 °N, the ages decrease due to the mixing with newly formed lower NADW in this region (Fig. 12, b and c, Fig. 13, a). The distribution of mean- and mode-ages also show a difference in the zonal direction. As shown in Fig.12 b and c, the general age distribution presents a trend with lower ages in the west, and higher in the east. Along the A10 section at 30 °S, the AABW has a mean-age of ~400 in the west and ~600 years in the east, whereas the mode-age is ~50 in the west and ~100 in the east. A similar situation is recorded along the A05 section; the mean-age of NEABW is ~600 years in the west and ~800 years in the east, whereas the mode-age is ~80 years in the west and between ~120 years in the east (Fig. 13, b). An additional factor that affects the age distributions is the mixing between AABW and NADW. In the south hemisphere, both ages are relatively low (~400 years for mean-age and ~80 years for mode-age) at the pressures below 4000 dbar, where the AABW has a fraction higher than 50%, while the ages are significantly higher when the AABW mixes with lower NADW at pressure of ~3000 dbar, especially in the region between 0 and 10 °W, the mean-age reaches up to ~800 years and the mode-age is ~120 years. This is because the “old” NADW takes up a fraction for more than 50% to 80%. The situation in the north hemisphere is the opposite, the ages of NEABW are higher in the bottom layer below 4000 dbar but lower in the deep layer at 3000 dbar due to the mixing with the young NADW. In the western basin, the mean-age is ~ 600 years and mode-age is ~80 years in the bottom, while ~400 years and ~50 years when mixes with NADW. Similar in the east basin, the mean-age is ~800 years and mode-age is ~120 years below 4000 dbar, while ~600 years and ~100 years at 3000 dbar (Fig. 13, b).

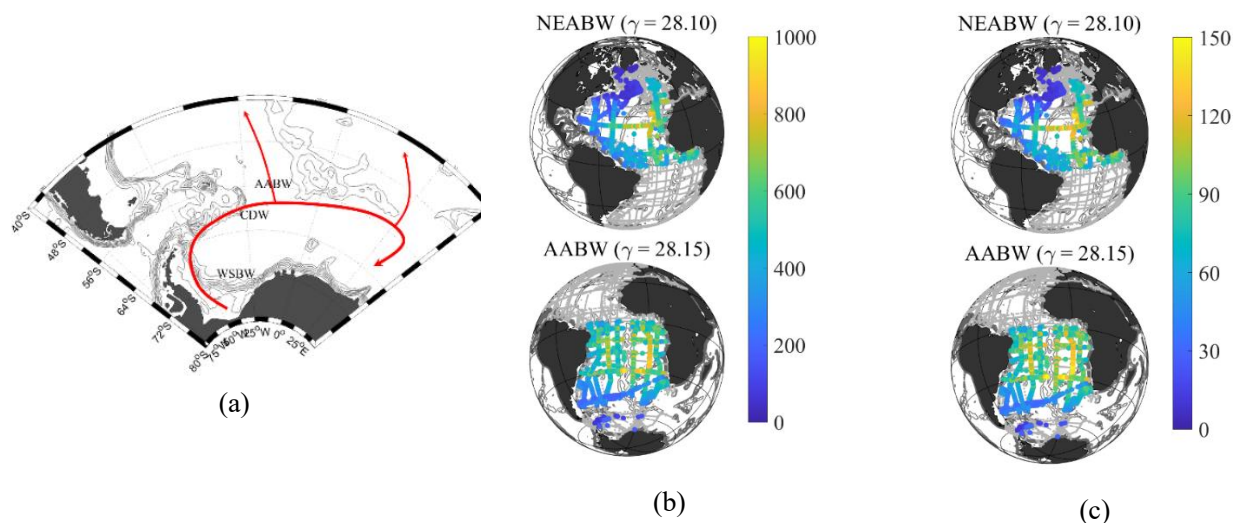


Figure 12. Ages of bottom water masses in the Atlantic Ocean.

(a) Main currents in the bottom layer. The currents (arrows) and the formation areas (rectangular shadows) of water masses in the deep and overflow layer.

(b) The mean- and (c) mode-ages of bottom water masses at their core neutral densities (kg m^{-3}). The colored dots show the ages in each station. The grey dots show all the GLODAPv2 stations that have less than 20% contribution of the water mass in question or lack of transient-tracer data.

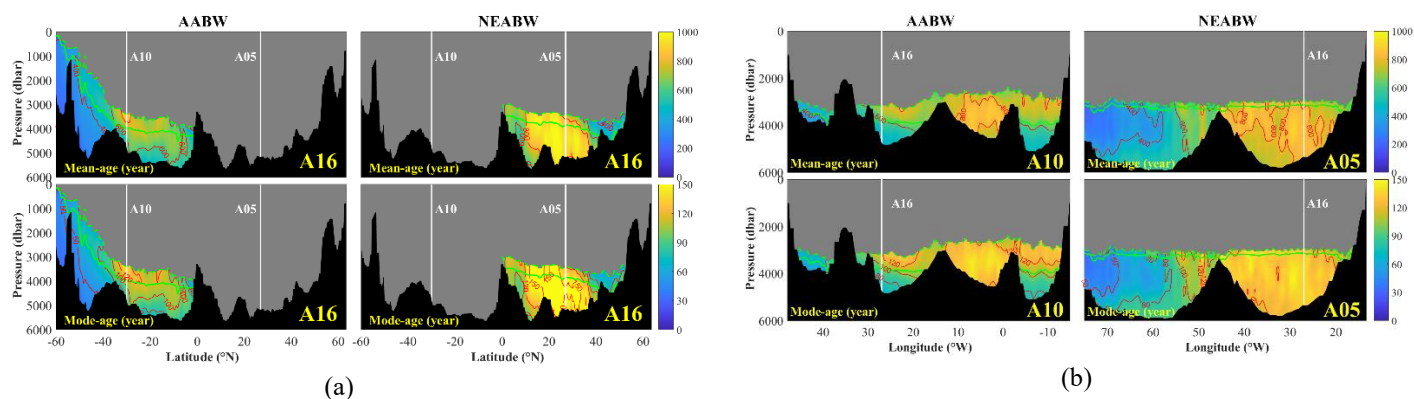


Figure 13. Mean-ages of AABW and NEABW along the A16 (a), A05 and A10 (b) section lines.

The green contour lines show fractions of water masses in 50 and the dashed green lines show the 20 % fractions. The grey blank indicates less than 20% contribution from bottom water masses. The white vertical lines show cross overs with other section lines.



4 The application of water mass ages in estimating the oxygen utilization rate (OUR)

The oxygen concentration in seawater under steady state is maintained by the balance of supply from oxygen-rich surface water and consumption by the respiration of organic matter. The Apparent Oxygen Utilization (AOU) shows the accumulated oxygen consumption in a water mass since isolated from the atmosphere, and is defined as the difference between saturated and measured oxygen concentration (i.e. $AOU = O_{\text{O}_2\text{sat}} - O_{\text{O}_2\text{meas}}$, Redfield, 1942; Redfield et al., 1963; Pytkowicz, 1971). The Oxygen Utilization Rate OUR ($\mu\text{mol kg}^{-1} \text{ yr}^{-1}$) can be calculated from AOU and water mass age and shows the integrated oxygen utilization rate (oxidation rate) during the pathway of a water mass from surface of the formation area to the sampling location (Jenkins, 1987; Doney and Bullister, 1992; Sonnerup et al., 2013). In addition, the OUR is also an important indicator in characterizing the combination of ventilation and respiration of the interior ocean (Koeve and Kähler, 2016; Thomas et al., 2020).

The true, or local OUR is difficult to estimate, and the main difficulty focuses on the determination of the “true” water mass age since the seawater comes from different pathways due to the mixing in the ocean interior (Tomczak, 1999; Koeve and Kähler, 2016). Researchers have tried a variety of ways to define the age of a water mass. For instance, the tracer-age (CFC age) is used in Karstensen et al., (2008), while the mean-age (partial pressure ages) is used in Sonnerup et al., (2015) in estimating the “integrated” water mass age that effects the oxygen consumption. As described in Section 2.2, the mean-age represents the average of all the parts in one water sample, so the OUR calculated from mean-age is a “mixed” value of all the contributing water masses in the sample. In the steady state, the mean-age can reflect the “mixed” or “integrated” OUR objectively. However, when we are labelling a specific wide-spread water mass and investigating the transport time from formation area, this water mass is often mixed with the surrounding water masses, so the mean-age reflects the “mixed” OUR of the mixture instead of the original labelling water mass. In this case, the mode-age is a better choice, because it describes the dominant time-scale a specific water mass takes from surface of formation area to the pressure of sampling place. In other words, the mode age is closer to the transport time of the original water mass and the OUR calculated from the mode-age might be a reasonable representation of the average OUR during the transport to the sampling location. In this section, we focus on the wide-spread water masses in the Atlantic Ocean and the mode-age is used to calculate the OUR during the active transport of wide-spread water masses.

Water masses with mode-ages larger than ~50 years in some parts of their distribution, including the AAIW, NADW, AABW and NEABW in the Atlantic Ocean, are defined here as wide-spread water masses. The transports of these wide-spread water masses are significantly influenced by the currents and topography. Therefore, their mode-age shows regional differences. Such differences also exist in DO and AOU, and lead to the spatial differences in OUR, especially between the eastern and western basins (Fig. 14). In the meridional direction, the mode-age increases with the distance from formation area. In the zonal direction, significant differences exist between the east and west of MAR. The wide-spread water masses generally have lower mode-ages in the western basin, which is better ventilated by the WBC and the DWBC (Fig. 14, left). In addition, surface oxygen-rich water is transported by these water masses to the deeper layers and are gradually consumed during the path-way. As a result, the DO is highest in the formation area and decreases with the distance. Meanwhile, the western basin displays higher DO due to the better ventilation (Fig. 14, middle left). The OUR shows a similar distribution to DO indicating that higher oxygen consumption rate, or oxidation rate is co-located with the regions with high oxygen concentration. At the same time, Fig. 14 also shows that the OUR approaches 0 when the mode-age is larger than ~50 years.

In the intermediate layer, the AAIW show low mode-ages, high DO and low AOU in the formation area near the Antarctic region. During the northward transport between 40 °S and 20 °N, the mode-ages increase and the DOs decrease with distance from the formation area (Fig. 14, upper panel). In general, the mode-ages are lower in the west, while the zonal difference for



DOs are not significant except for some regions in the eastern basins. The mode-ages are mostly between ~60 and ~90 years and reaches up to ~120 years in the poor ventilated eastern basin. The DOs are between 160 and 220 $\mu\text{mol kg}^{-1}$ in the south hemisphere and mostly between 100 and 160 $\mu\text{mol kg}^{-1}$ in the north hemisphere. The OURs in the Antarctic region obtain the highest value in the latitude region between 20 and 40 °S and decrease on the pathway to the north until 20 °N.

In the deep and overflow layer, the NADW is newly formed in the high north latitude. In most regions covered by the NADW between 30 °N and 40 °S, the differences between west and east exist with obvious low mode-age and AOU (high DO) and in the west, where is well ventilated by the DWBC (Fig. 14). The mode-age is between ~30 and ~60 years in the west and between ~90 and ~150 years in the east. The AOU is lower in the west and higher in the east. The OUR, which shows the opposite distribution as the AOU in the zonal direction, obtains the highest value in the formation area of NADW, maintains relative higher in the west along the DWBC region and shows a lower value in the eastern basin.

The bottom layer is occupied by the AABW and NEABW in the south and north hemisphere respectively. The AABW is formed in the Antarctic region with an original mode-age lower than ~30 years and increases on the way to the north. Similar to the AAIW and NADW, the western basin is better ventilated, therefore the mode-ages are lower in the west at the same latitude (Fig. 14, lower panel). In contrast to the AAIW and NADW, the AABW obtains relative lower DOs and higher AOU when formed (see also Fig. 15, b). In the western basin of the South Atlantic, the DOs decrease to 220 $\mu\text{mol kg}^{-1}$ and the AOU increase to 130 $\mu\text{mol kg}^{-1}$ on the pathway, while in the eastern basin, the DOs are 240 $\mu\text{mol kg}^{-1}$ and the AOUs are 110 $\mu\text{mol kg}^{-1}$. This is because the eastern basin is more influenced by the relative oxygen-rich NADW from the north. Similarly, the DOs and AOU of NEABW in the North Atlantic also show similar states to the NADW. In west regions ventilated by the DWBC, the DOs reach the values of higher than 260 $\mu\text{mol kg}^{-1}$ and AOU is lower than 70 $\mu\text{mol kg}^{-1}$. This result can also be confirmed in Figure 15. Although the distributions of DOs and AOU are more complex in the bottom layer, the OURs still match the distribution of mode-ages. The highest OURs appears in the formation area near the Antarctic region with values higher than 4 $\mu\text{mol kg}^{-1} \text{ yr}^{-1}$. In the western Atlantic region with low mode-ages, the OURs show relative higher values (> between 1 and 3 $\mu\text{mol kg}^{-1} \text{ yr}^{-1}$) and low value (below 1 $\mu\text{mol kg}^{-1} \text{ yr}^{-1}$) in the east (Fig. 14, lower panel).

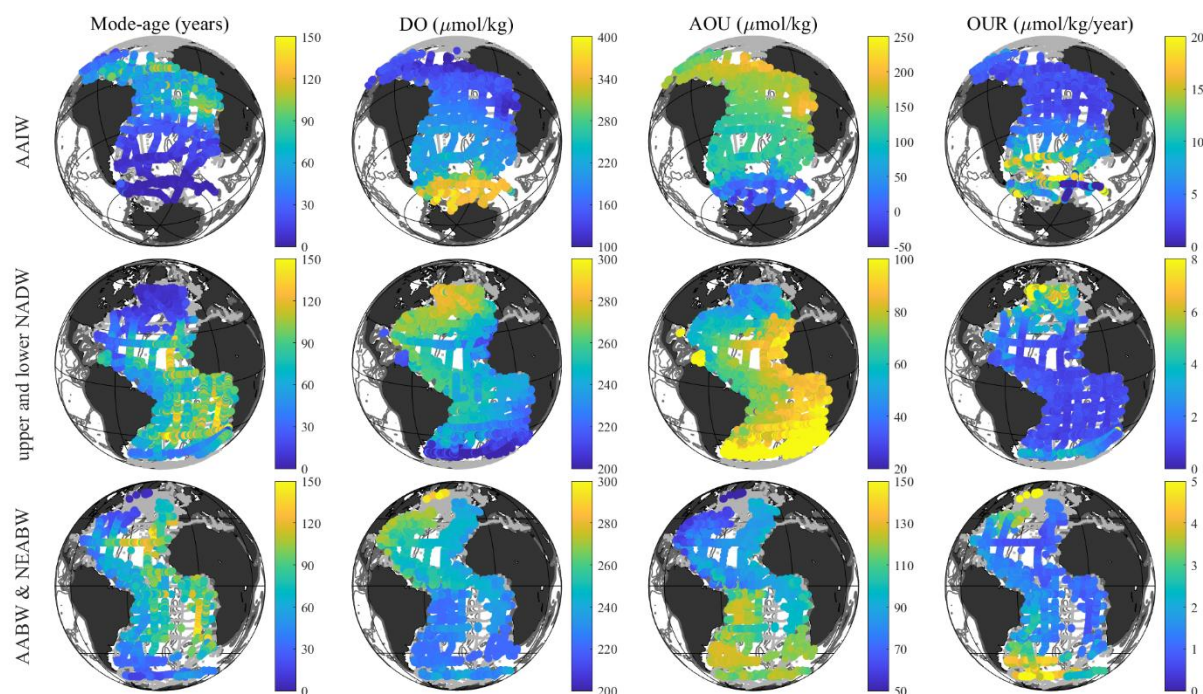


Figure 14. Mode-age, DO, AOU and OUR of wide-spread water masses in the Atlantic Ocean.

The colored dots show the values in each station at core neutral densities of each water mass (AAIW at 27.20, upper NADW at 27.95, lower NADW at 28.05, AABW at 28.15, NEABW at 28.10 kg m^{-3} , the upper and lower NADW, AABW and NEABW are shown in one plot. The grey dots show all the GLODAPv2 stations that have less than 20% contribution of the water mass in question.

405 The above four properties are also represented along the A16 section (Fig. 15). The AAIW has the lowest mode-age among
 406 the three water masses, but also the largest variations in the DO and AOU. The mode-age indicates that in total of ~40 to 60
 407 years is needed for the main body of AAIW (fractions > 80%) to be transported to the equator (Fig 15, a). The DO decreases
 408 rapidly from 260 to below 180 $\mu\text{mol kg}^{-1}$ at the oxygen minimum zone at 20 °S, while the AOU increases from 60 to 150 μmol
 409 kg^{-1} during the northward pathway (Fig 15, b and c). The OUR is higher than 8 $\mu\text{mol kg}^{-1} \text{yr}^{-1}$ at the beginning and decreases
 410 to 3 $\mu\text{mol kg}^{-1} \text{yr}^{-1}$ close to the equator (Fig 15, d). The mode-age of NADW is ~140 years at 40 °S and reaches a peak of ~160
 411 years in the region of 20 °N due to the sluggish water exchange caused by the topography. The NADW contains the highest
 412 oxygen concentration and the lowest AOU and OUR in the abyssal Atlantic Ocean. The value of DO is 260 $\mu\text{mol kg}^{-1}$ at the
 413 starting point at 60 °N and still remains 220 $\mu\text{mol kg}^{-1}$ at 40 °S where it meets the AABW and AAIW. The AOU of NADW
 414 remains below 100 $\mu\text{mol kg}^{-1}$ during the entire pathway. The OUR of NADW is below 5 $\mu\text{mol kg}^{-1} \text{yr}^{-1}$ close to the formation
 415 area, and below 1 $\mu\text{mol kg}^{-1} \text{yr}^{-1}$ south of 60 °N. The transport of the main body of AABW takes in total of ~100 years from
 416 the Weddell Sea to the equator. The DO and AOU remain unchanged at 220 and 130 $\mu\text{mol kg}^{-1}$ respectively on the pathway to
 417 the equator, indicating very low OUR. Although derived from the AABW, the characteristics of the NEABW are more similar
 418 to the NADW in all the above properties.

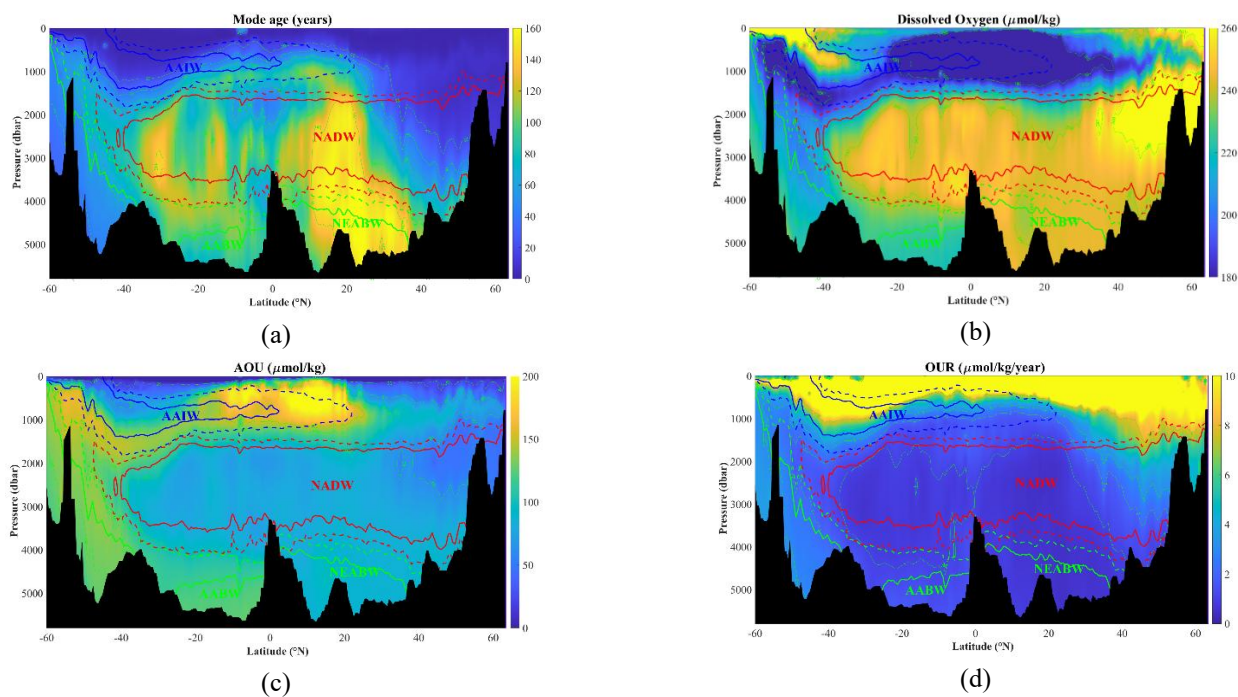


Figure 15. Distributions of mode-age (a), dissolved oxygen (b), conservative temperature (c) and AOU (d) along the A16 section line. The color solid lines show the fractions of 80% in each water mass and the dashed lines show the fractions of 50%.



5 Estimation of water mass ages based on ^{39}Ar

As a representative of noble gas radionuclides, ^{39}Ar is considered to exhibit nearly ideal chemical and physical properties for studying earth and environmental processes (Lu et al., 2014). In this study, the mean- and mode- ages of Atlantic wide-spread water masses, including AAIW, NADW, AABW, and NEABW, are also estimated based on observations of ^{39}Ar . For this purpose, we make a distinction between the western (green dots) and eastern (red dots) Atlantic, divided by the Mid-Atlantic-Ridge (Fig. 16a). The distribution of ^{39}Ar is shown in Fig. 16 b. Near the formation area of each wide-spread water mass, the concentration of ^{39}Ar approaches approximately 100%, indicating that the surface waters are in equilibrium with the atmosphere. As these water masses are transported over long distances and extended periods, the continuous decay of ^{39}Ar leads to concentrations decreasing to roughly 30% at their furthest locations. By integrating this information with its half-life of 269 years, the water mass ages can be estimated. For ^{39}Ar we focus our attention to the older water masses, as the younger ones are better characterized by CFC12 and SF_6 .

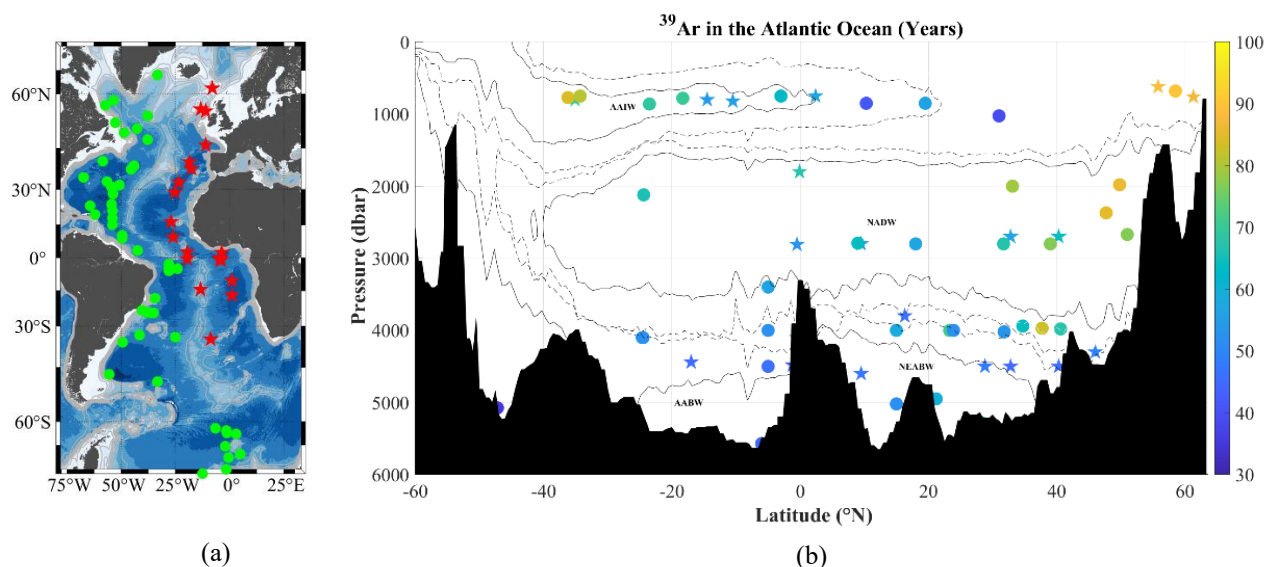


Figure 16. (a) Map of the ^{39}Ar sampling stations. The green circle dots show the stations in the west Atlantic Ocean (west of M-A-R), while the red pentagrams show the stations in the east Atlantic Ocean. (b) Distributions of ^{39}Ar in the Atlantic Ocean (% Modern). The circle dots show the data in the west, while the pentagrams show the data in the east Atlantic Ocean. The solid isolines show the 50% fractions of water masses and the dashed lines show the 20 % fractions.

Similar to the findings from CFC-12 and SF_6 observations, the mean- and mode-ages derived from measurements using ^{39}Ar increase with transport from the source of formation (Fig. 17). At a latitude of approximately 40°S , the AAIW exhibits mean-ages ranging between ~ 100 to ~ 200 years (with mode-age around ~ 30 years). When transported northward to about 20°S , both mean- and mode-ages rise to roughly ~ 300 years and ~ 60 years respectively. Upon reaching approximately 10°N during further northward transport, these values escalate to around ~ 700 years for mean-age and ~ 100 years for mode-age. However, near the region at about 20°N , the terminus for northward flow, the mean-age decreases back down to roughly ~ 400 years while maintaining a mode-age close to ~ 60 years due to mixing with younger upper NADW. In the deep and overflow layer, the newly formed NADW initiates at high northern latitudes, exhibiting both mean- and mode-ages approaching zero. During southward transport at around 30°S , the concentration data indicates corresponding mean- and mode-ages of approximately ~ 400 years and ~ 60 years respectively. Similarly, the bottom water masses (AABW and NEABW) display mean- and mode-



ages of around ~500 years and ~100 years respectively at the farthest end of the transport distance approximately 50 °N.

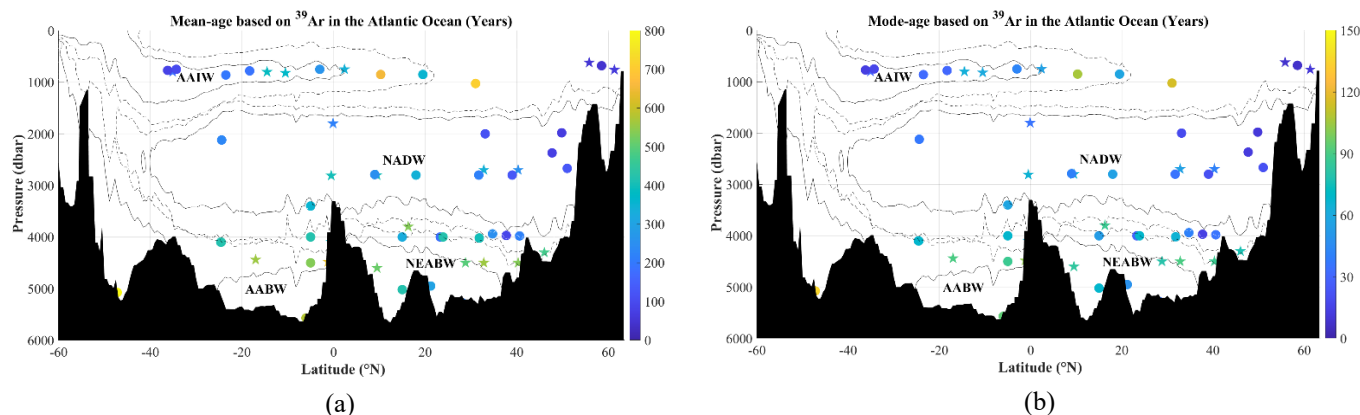


Figure 17. Mean- (a) and mode-ages (b) of the wide-spread water masses estimated by ^{39}Ar in the Atlantic Ocean. The circle dots show the data in the west, while the pentagrams show the data in the east Atlantic Ocean. The solid isolines show the 50% fractions of water masses and the dashed lines show the 20 % fractions.

The contrast between the western and eastern Atlantic Ocean is distinctly evident (Fig. 18). Generally, higher concentrations of ^{39}Ar are observed in the west compared to the east at equivalent latitudes. For instance, in the vicinity of the AAIW formation area at 40 °S, the ^{39}Ar concentration is approximately 100% in the west and around 70% in the east. In the intermediate layer near the equator, these concentrations decrease to about 70% (west) and 50% (east). These findings suggest that both mean- and mode-ages of AAIW are close to zero at 40 °S. The mean-age is estimated to be ~300 years in the west and ~500 years in the east. Similar results are also observed in the deep water and overflow layers. Based on elevated levels of ^{39}Ar near its formation area, it can be inferred that both mean- and mode-ages of NADW are close to zero at 60 °N across both West and East Atlantic Oceans. Between 20 °N and the equator, the mean-age is estimated to be ~300 years in the west and ~500 years in the east; while the mode-age is around ~60 years (west) and ~90 years (east), respectively. For bottom water masses below a depth of 4000 m, concentrations of ^{39}Ar generally fall below 50%, with higher levels observed in the west (50%-60%) compared to lower levels seen in the east (40%-50%) between 20 °S and 40 °N, indicating the water mass ages range from ~400–500 years (mean-age) and ~60–90 years (mode-age) in the west, and from ~500–600 years (mean-age) and ~90–120 years (mode-age) in the east.

As expected, there are differences in the inferred age of water masses depending on which tracer you use. Apart from a possible mis-representation of the TTD by the IG distribution, this is due to different validity ranges for the three tracers. The mean- and mode-ages based on ^{39}Ar are generally lower than those based on CFC-12 and SF_6 , and such difference increases with the age of the water mass. For instance, in the eastern basin near 20 °N, the mean-age of NADW is ~1000 years and the mode-age is ~150 years by using CFC-12 and SF_6 (Fig. 10 and 11), whereas both ages are ~600 (mean) and ~90 (mode) years when based on ^{39}Ar (Fig. 17). Similarly, the mean- and mode-ages of the AABW (NEABW) near 50 °N are ~800 and ~120 years (Fig. 12 and 13), respectively, based on CFC-12 and SF_6 , but ~500 and ~100 years based on ^{39}Ar . The low concentrations of CFC-12 and SF_6 in the deep water can induce the increase of error and lead to an over-estimated water mass ages, and the ages derived from ^{39}Ar are better estimates. However, due to the insufficient number of sampling data for ^{39}Ar , it is not possible to form a cross-section plot. From the aforementioned differences, it is evident that the correct selection of tracers is also crucial for accurately determining the age of the water mass.



466 6 Conclusions and discussion

467 The geographic distributions of main water masses in the Atlantic Ocean are reported in Liu and Tanhua, (2021). As the
468 continuous work, the transports of water masses are traced by the transient tracers (CFC-12 and SF₆) and the water mass ages
469 (consuming time during the pathway) are estimated. The assumption of a standard mixing ratio ($\Delta/\Gamma = 1$) and a saturation of
470 100% is followed. Three different definitions of water mass ages are investigated. The tracer-age assumes the ocean as a totally
471 advective situation without diffusion and underestimates the actual age in the realistic ocean. The mean-age, which shows the
472 average value of all the different parts in one water sample, is used to show the static distribution of water masses. The mode-
473 age, which shows the age of the dominant water mass in the sample, is used to trace the biogeochemical phenomena.

474 In general, the water mass age increases with the pressure and distance from the formation area, so the central waters in the
475 upper layer obtain the lowest ages of within ~100 years. In the intermediate layer, the AAIW and MW are two conspicuous
476 water masses and both take ~300 years to spread from south to north (AAIW) and east to west (MW) respectively. As the
477 dominant water mass in the deep and overflow layer, the NADW takes ~500 years to spread along the DWBC in the west
478 Atlantic Ocean, and takes ~ 900 years eastward to cover the east part. The bottom waters origin from south of Antarctic
479 Circumpolar Current region take ~600 years to spread northward and cover the bottom layer. Similar as the NADW, the mean-
480 age of both AABW and NEABW show spatial difference between the west (low mean-age) and the east (high mean-age). This
481 is because the west Atlantic Ocean is well ventilated by the DWBC while the water exchange is sluggish in the east.

482 The transient tracers (CFC-12, SF₆ and ³⁹Ar), serve as effective tools for identifying and quantifying oceanographic ventilation,
483 each tracer possessing distinct advantages and limitations in determining and tracing the depths and mean ages of water masses.
484 CFC-12 and SF₆ exhibit optimal applicability for water masses range within 2000 dbar pressure (or mean-ages < ~500 years).
485 However, their utility becomes constrained in deeper aqueous regimes (below 2000 dbar or mean-age > ~500 years) due to
486 inherent limitations in tracer concentration sensitivity, which may induce systematic overestimations of water mass ages when
487 applied to deep or bottom layers. The chemically inert radioisotope ³⁹Ar, characterized by a 269-year half-life, effectively
488 addresses this observational gap through its unique temporal resolution. Consequently, the synergistic application of SF₆, CFCs,
489 and ³⁹Ar in multi-tracer frameworks overcomes temporal constraints inherent to single-tracer approaches, enabling
490 comprehensive investigation of coupled biogeochemical-climate interactions. This integrated methodology facilitates novel
491 insights into climate-driven water mass reorganization, carbon cycle dynamics, and other critical marine processes essential
492 for understanding oceanic responses to global change.

493 The ventilations and respiration rates (oxidation rates, OUR) of wide-spread water masses are estimated by the mode-ages.
494 The currents and topography have significant impacts on the mode-ages and furthermore the the apparent oxygen utilisation
495 rate (OUR). The western basins of the Atlantic Ocean are better ventilated with lower the mode-ages, while the OURs show
496 the opposite distribution, suggesting that the mode-age is an important determinant of OUR in seawater than AOU and higher
497 respiration rates exist when the region is better ventilated.

498 The aim of this study was to investigate the age distribution of the Atlantic water mass and its impact on climate change. By
499 collecting a large amount of ocean observation data and using numerical simulation methods, we have conducted an in-depth
500 study of the formation, evolution and age of the Atlantic water mass. The results show that with global warming, the age of
501 the Atlantic water mass shows a certain degree of change. In particular, the Arctic region has been significantly affected by
502 the melting of ice caps and other factors. In addition, we also found that there are complex interactions between different water
503 masses, which has important implications for predicting future climate change.



504 In summary, this study reveals the close relationship between the age distribution of Atlantic water mass and climate change,
505 and provides an important reference for further understanding of ocean circulation systems. It is hoped that this study can
506 provide useful information for scientists and policy makers in related fields, and promote more in-depth discussion on climate
507 change and the formulation of countermeasures on a global scale.

508 **Author contributions.** ML designed the research study and conducted the analysis. ML and TT interpreted the results and
509 wrote the paper.

510 **Competing interests.** The contact author has declared that none of the authors has any competing interests.

511 Acknowledgements

512 This work is based on the comprehensive and detailed data from the GLODAP data product throughout the past few decades.
513 In particular, we are grateful to the efforts from all the scientists and crews on cruises, who generated funding and dedicated
514 time on committing the collection of data. We also would like to thank the working groups of GLODAP for their support and
515 information of the collation, quality control and publishing of data. Their contributions and selfless sharing are prerequisites
516 for the completion of this work. In addition, we are grateful to Dr. Tim Stöven for his support and advices in running calculating
517 programs of water mass ages. Thanks goes to Prof. Minggang Cai and his research group at the College of Ocean and Earth
518 Sciences, Xiamen University for the help and support during Mian Liu's postdoctoral work, also goes to all the colleagues in
519 School of Environmental Science and Engineering, Xiamen University of Technology.

520 **Financial support.** The authors gratefully thank the Research Start-up Project for the Introduction (Cultivation) of High-level
521 Talents of Xiamen University of Technology (No. YKJ23021R), National Natural Science Foundation of China (No. 22106128)
522 and the Xiamen University of Technology National Natural Science Foundation of China Training Programme for Excellence
523 (No. XPYM2409). Mian Liu received support from the China Scholarship Council (CSC) to support the PhD study at
524 GEOMAR Helmholtz Centre for Ocean Research Kiel.



525 References

- 526 Armour, K. C., J. Marshall, J. R. Scott, A. Donohoe, and E. R. Newsom: Southern Ocean warming delayed by circumpolar
527 upwelling and equatorward transport, *Nature Geoscience*, 9(7), 549-554, doi:10.1038/ngeo2731, 2016.
- 528 Bender, M. L.: The $\delta^{18}\text{O}$ of dissolved O_2 in seawater: A unique tracer of circulation and respiration in the deep sea, *Journal of*
529 *Geophysical Research: Oceans*, 95(C12), 22243-22252, doi:<https://doi.org/10.1029/JC095iC12p22243>, 1990.
- 530 Bjerknes, J.: Atlantic Air-Sea Interaction, in *Advances in Geophysics*, edited by H. E. Landsberg and J. Van Mieghem, pp. 1-
531 82, Elsevier, doi:[https://doi.org/10.1016/S0065-2687\(08\)60005-9](https://doi.org/10.1016/S0065-2687(08)60005-9), 1964.
- 532 Bryden, H. L., H. R. Longworth, and S. A. Cunningham: Slowing of the Atlantic meridional overturning circulation at 25
533 degrees N, *Nature*, 438(7068), 655-657, doi:10.1038/nature04385, 2005.
- 534 Bullister, J. L., and R. F. Weiss: Anthropogenic Chlorofluoromethanes in the Greenland and Norwegian Seas, *Science*,
535 221(4607), 265-268, doi:10.1126/science.221.4607.265, 1983.
- 536 Bullister, J. L., D. P. Wisegarver, and F. A. Menzia: The solubility of sulfur hexafluoride in water and seawater, *Deep Sea*
537 *Research Part I: Oceanographic Research Papers*, 49(1), 175-187, doi:10.1016/s0967-0637(01)00051-6, 2002.
- 538 Clark, P. U., J. D. Shakun, P. A. Baker, P. J. Bartlein, S. Brewer, E. Brook, A. E. Carlson, H. Cheng, D. S. Kaufman, and Z.
539 Liu: Global climate evolution during the last deglaciation, *Proceedings of the National Academy of Sciences*, 109(19), E1134-
540 E1142, doi:10.1073/pnas.1116619109, 2012.
- 541 Dickson, R. R., and J. Brown: The production of North Atlantic Deep Water: Sources, rates, and pathways, *Journal of*
542 *Geophysical Research: Oceans*, 99(C6), 12319-12341, doi:10.1029/94jc00530, 1994.
- 543 Doney, S. C., and J. L. Bullister: A chlorofluorocarbon section in the eastern North Atlantic, *Deep-Sea Res*, 39(11-12A), 1857-
544 1883, doi:10.1016/0198-0149(92)90003-c, 1992.
- 545 Fine, R. A.: Observations of CFCs and SF_6 as Ocean Tracers, in *Annual Review of Marine Science*, Vol 3, edited by C. A.
546 Carlson and S. J. Giovannoni, pp. 173-195, doi:10.1146/annurev.marine.010908.163933, 2011.
- 547 Gammon, R. H., J. Cline, and D. Wisegarver: Chlorofluoromethanes in the northeast Pacific Ocean: Measured vertical
548 distributions and application as transient tracers of upper ocean mixing, *Journal of Geophysical Research-Oceans*, 87(NC12),
549 9441-9454, doi:10.1029/JC087iC12p09441, 1982.
- 550 Hall, M. M., and H. L. Bryden: Direct Estimates and Mechanisms of Ocean Heat-Transport, *Deep-Sea Res*, 29(3), 339-359,
551 doi:10.1016/0198-0149(82)90099-1, 1982.
- 552 Hall, T. M., and R. A. Plumb: Age as a diagnostic of stratospheric transport, *Journal of Geophysical Research-Atmospheres*,
553 99(D1), 1059-1070, doi:10.1029/93jd03192, 1994.
- 554 Huhn, O., M. Rhein, M. Hoppema, and S. van Heuven: Decline of deep and bottom water ventilation and slowing down of
555 anthropogenic carbon storage in the Weddell Sea, 1984-2011, *Deep Sea Research Part I: Oceanographic Research Papers*, 76,



- 556 66-84, doi:10.1016/j.dsr.2013.01.005, 2013.
- 557 Ito, T., A. Nenes, M. S. Johnson, N. Meskhidze, and C. Deutsch: Acceleration of oxygen decline in the tropical Pacific over
558 the past decades by aerosol pollutants, *Nature Geoscience*, 9(6), 443-447, doi:10.1038/ngeo2717, 2016.
- 559 Jenkins, W. J.: Oxygen utilization rates in North Atlantic subtropical gyre and primary production in oligotrophic systems,
560 *Nature*, 300(5889), 246-248, doi:10.1038/300246a0, 1982.
- 561 Jenkins, W. J.: ^3H and ^3He in the Beta Triangle: Observations of Gyre Ventilation and Oxygen Utilization Rates, *Journal of*
562 *Physical Oceanography*, 17(6), 763-783, doi:10.1175/1520-0485(1987)017<0763:Aitbto>2.0.Co;2, 1987.
- 563 Jia, Z.-H., P. Zhang, L.-B. Li, Q.-W. Chen, J.-L. Liu, Y.-G. Liu, Q. Wu, Y. Yang, L.-T. Sun G.-M. Yang, W. Jiang, Z.-T. Lu:
564 Stability and reliability study of an ^{39}Ar enrichment system for accurate ^{39}Ar dating, *Nuclear Instruments and Methods in*
565 *Physics Research Section A: Accelerators, Spectrometers, Detectors and Associated Equipment*, 1075, 170438,
566 doi:<https://doi.org/10.1016/j.nima.2025.170438>, 2025.
- 567 Karstensen, J., and M. Tomczak, Ventilation processes and water mass ages in the thermocline of the southeast Indian Ocean,
568 *Geophysical Research Letters*, 24(22), 2777-2780, doi:10.1029/97gl02708, 1997.
- 569 Karstensen, J., and M. Tomczak: Age determination of mixed water masses using CFC and oxygen data, *Journal of Geophysical*
570 *Research-Oceans*, 103(C9), 18599-18609, doi:10.1029/98jc00889, 1998.
- 571 Karstensen, J., L. Stramma, and M. Visbeck: Oxygen minimum zones in the eastern tropical Atlantic and Pacific oceans,
572 *Progress in Oceanography*, 77(4), 331-350, doi: 10.1016/j.pocean.2007.05.009, 2008.
- 573 Kirchner, K., M. Rhein, S. HuttI-Kabus, and C. W. Böning: On the spreading of South Atlantic Water into the Northern
574 Hemisphere, *Journal of Geophysical Research-Oceans*, 114, doi:10.1029/2008jc005165, 2009.
- 575 Koeve, W., and P. Kähler: Oxygen utilization rate (OUR) underestimates ocean respiration: A model study, *Global*
576 *Biogeochemical Cycles*, 30(8), 1166-1182, doi:10.1002/2015gb005354, 2016.
- 577 Kuhlbrodt, T., A. Griesel, M. Montoya, A. Levermann, M. Hofmann, and S. Rahmstorf: On the driving processes of the Atlantic
578 meridional overturning circulation, *Reviews of Geophysics*, 45(1), doi:10.1029/2004rg000166, 2007.
- 579 Lauvset, S. K., R. M. Key, A. Olsen, S. van Heuven, A. Velo, X. Lin, C. Schirnack, A. Kozyr, T. Tanhua, M. Hoppema, S.
580 Jutterström, R. Steinfeldt, E. Jeansson, M. Ishii, F. F. Pérez, T. Suzuki and S. Watelet. A new global interior ocean mapped
581 climatology: the 1°x1° GLODAP version 2, *Earth Syst. Sci. Data*, 8, 325–340, <https://doi.org/10.5194/essd-8-325-2016>, 2016.
- 582 Lauvset, S. K., Lange, N., Tanhua, T., Bittig, H. C., Olsen, A., Kozyr, A., Álvarez, M., Azetsu-Scott, K., Brown, P. J., Carter,
583 B. R., Cotrim da Cunha, L., Hoppema, M., Humphreys, M. P., Ishii, M., Jeansson, E., Murata, A., Müller, J. D., Pérez, F. F.,
584 Schirnack, C., Steinfeldt, R., Suzuki, T., Ulfsbo, A., Velo, A., Woosley, R. J., and Key, R. M.: The annual update
585 GLODAPv2.2023: the global interior ocean biogeochemical data product, *Earth Syst. Sci. Data*, 16, 2047–2072,
586 <https://doi.org/10.5194/essd-16-2047-2024>, 2024.
- 587 Liu, M., and T. Tanhua: Water masses in the Atlantic Ocean: characteristics and distributions, *Ocean Science*, 17(2), 463-486,



588 doi:10.5194/os-17-463-2021, 2021.

589 Maiss, M., L. P. Steele, R. J. Francey, P. J. Fraser, R. L. Langenfelds, N. B. A. Trivett, and I. Levin: Sulfur hexafluoride - A
590 powerful new atmospheric tracer, *Atmospheric Environment*, 30(10-11), 1621-1629, doi:10.1016/1352-2310(95)00425-4,
591 1996.

592 Morrison, A. K., T. L. Frolicher, and J. L. Sarmiento: Upwelling in the Southern Ocean, *Physics Today*, 68(1), 27-32,
593 doi:10.1063/pt.3.2654, 2015.

594 Olsen, A., R. M. Key, S. van Heuven, S. K. Lauvset, A. Velo, X. Lin, C. Schirnick, A. Kozyr, T. Tanhua, M. Hoppema, S.
595 Jutterström, R. Steinfeldt, E. Jeansson, M. Ishii, F. F. Pérez and T. Suzuki. The Global Ocean Data Analysis Project version 2
596 (GLODAPv2) – an internally consistent data product for the world ocean, *Earth Syst. Sci. Data*, 8, 297–
597 323, <https://doi.org/10.5194/essd-8-297-2016>, 2016.

598 Orsi, A. H., G. C. Johnson, and J. L. Bullister: Circulation, mixing, and production of Antarctic Bottom Water, *Progress in*
599 *Oceanography*, 43(1), 55-109, doi:10.1016/s0079-6611(99)00004-X, 1999.

600 Patara, L., C. W. Böning, and T. Tanhua: Multidecadal Changes in Southern Ocean Ventilation since the 1960s Driven by Wind
601 and Buoyancy Forcing, *Journal of Climate*, 34(4), 1485-1502, doi:10.1175/Jcli-D-19-0947.1, 2021.

602 Purkey, S. G., and G. C. Johnson: Warming of Global Abyssal and Deep Southern Ocean Waters between the 1990s and 2000s:
603 Contributions to Global Heat and Sea Level Rise Budgets, *Journal of Climate*, 23(23), 6336-6351, doi:10.1175/2010jcli3682.1,
604 2010.

605 Pytkowicz, R. M.: On the apparent oxygen utilization and the preformed phosphate in the oceans¹, *Limnology and*
606 *Oceanography*, 16(1), 39-42, <https://doi.org/10.4319/lo.1971.16.1.0039>, 1971.

607 Rahmstorf, S.: The Great Ocean Conveyor: Discovering the Trigger for Abrupt Climate Change, *Nature*, 464(7289), 681-681,
608 doi:10.1038/464681a, 2010.

609 Redfield, A. C.: The processes determining the concentration of oxygen, phosphate and other organic derivatives within the
610 depths of the Atlantic Ocean, *Pap. Phys. Oceanogr. Meteorol. Mass. Inst. Technol. Woods Hole Oceanogr. Inst.*, 9, 1–22,
611 <https://doi.org/10.1575/1912/1053>, 1942.

612 Redfield, A. C., B. H. Ketchum, F. A. Richards, The influence of organisms on the composition of seawater, *The Sea. Ideas*
613 *and Observations on Progress in the Study of the Seas* M. N. Hill, 26–77, John Wiley, New York, 1963.

614 Sandström, J. W.: Dynamische versuche mit meerwasser. *Annalen der Hydrographie und Maritimen Meteorologie*, 36, 6–23,
615 1908.

616 Sandström, J. W.: Meteorologische studien im Schwedischen Hochgebirge. Göteborgs Kungl. Vetenskaps- och
617 Vitterhetssamhälles Handlingar, 17, 1–48, 1916.

618 Schmidtko, S., L. Stramma, and M. Visbeck: Decline in global oceanic oxygen content during the past five decades, *Nature*,
619 542(7641), 335-339, doi:10.1038/nature21399, 2017.



- 620 Schneider, A., T. Tanhua, A. Kortzinger, and D. W. R. Wallace: High anthropogenic carbon content in the eastern Mediterranean,
621 Journal of Geophysical Research-Oceans, 115, doi:10.1029/2010jc006171, 2010.
- 622 Skinner, L. C., F. Primeau, E. Freeman, M. de la Fuente, P. A. Goodwin, J. Gottschalk, E. Huang, I. N. McCave, T. L. Noble,
623 and A. E. Scrivner: Radiocarbon constraints on the glacial ocean circulation and its impact on atmospheric CO₂, Nature
624 Communications, 8, doi:10.1038/ncomms16010, 2017.
- 625 Sonnerup, R. E., S. Mecking, and J. L. Bullister: Transit time distributions and oxygen utilization rates in the Northeast Pacific
626 Ocean from chlorofluorocarbons and sulfur hexafluoride, Deep-Sea Res Pt I, 72, 61-71, doi:10.1016/j.dsr.2012.10.013, 2013.
- 627 Sonnerup, R. E., S. Mecking, J. L. Bullister, and M. J. Warner: Transit time distributions and oxygen utilization rates from
628 chlorofluorocarbons and sulfur hexafluoride in the Southeast Pacific Ocean, Journal of Geophysical Research-Oceans, 120(5),
629 3761-3776, doi:10.1002/2015jc010781, 2015.
- 630 Stanley, R. H. R., S. C. Doney, W. J. Jenkins, and D. E. Lott: Apparent oxygen utilization rates calculated from tritium and
631 helium-3 profiles at the Bermuda Atlantic Time-series Study site, Biogeosciences, 9(6), 1969-1983, doi:10.5194/bg-9-1969-
632 2012, 2012.
- 633 Stöven, T., and T. Tanhua: Ventilation of the Mediterranean Sea constrained by multiple transient tracer measurements, Ocean
634 Science, 10(3), 439-457, doi:10.5194/os-10-439-2014, 2014.
- 635 Sverdrup, H. U.: The unity of the sciences of the sea, Sigma Xi Quarterly, 28(3), 105-115,
636 <https://www.jstor.org/stable/23049117>, 1940.
- 637 Talley, L.: Antarctic Intermediate Water in the South Atlantic, in The South Atlantic: Present and Past Circulation, edited by
638 G. Wefer, W. H. Berger, G. Siedler and D. J. Webb, pp. 219-238, Springer Berlin Heidelberg, Berlin, Heidelberg,
639 doi:10.1007/978-3-642-80353-6_11, 1996.
- 640 Talley, L.: Closure of the Global Overturning Circulation Through the Indian, Pacific, and Southern Oceans: Schematics and
641 Transports, Oceanography, 26(1), 80-97, doi:10.5670/oceanog.2013.07, 2013.
- 642 Talley, L., R. Feely, B. Sloyan, R. Wanninkhof, M. Baringer, J. Bullister, C. Carlson, S. Doney, R. Fine, and E. Firing, N.
643 Gruber, D.A. Hansell, M. Ishii, G.C. Johnson, K. Katsumata, R.M. Key, M. Kramp, C. Langdon, A.M. Macdonald, J.T. Mathis,
644 E.L. McDonagh, S. Mecking, F.J. Millero, C.W. Mordy, T. Nakano, C.L. Sabine, W.M. Smethie, J.H. Swift, T. Tanhua, A.M.
645 Thurnherr, M.J. Warner, and J.-Z. Zhang: Changes in ocean heat, carbon content, and ventilation: A review of the first decade
646 of GO-SHIP global repeat hydrography, Annual review of marine science, 8, 185-215, [https://doi.org/10.1146/annurev-marine-](https://doi.org/10.1146/annurev-marine-052915-100829)
647 052915-100829, 2016.
- 648 Tamsitt, V., H. F. Drake, A. K. Morrison, L. D. Talley, C. O. Dufour, A. R. Gray, S. M. Griffies, M. R. Mazloff, J. L. Sarmiento,
649 J. Wang, W. Weijs: Spiraling pathways of global deep waters to the surface of the Southern Ocean, Nature Communications,
650 8(1), 172, doi:10.1038/s41467-017-00197-0, 2017.
- 651 Tanhua, T., A. Biastoch, A. Kortzinger, H. Luger, C. Boning, and D. W. R. Wallace: Changes of anthropogenic CO₂ and CFCs
652 in the North Atlantic between 1981 and 2004, Global Biogeochemical Cycles, 20(4), doi:10.1029/2006gb002695, 2006.



- 653 Tanhua, T., D. W. Waugh, and D. W. R. Wallace: Use of SF₆ to estimate anthropogenic CO₂ in the upper ocean, *Journal of*
654 *Geophysical Research-Oceans*, 113(C4), doi:10.1029/2007jc004416, 2008.
- 655 Tanhua, T., D. W. Waugh, and J. L. Bullister: Estimating changes in ocean ventilation from early 1990s CFC-12 and late 2000s
656 SF₆ measurements, *Geophysical Research Letters*, 40(5), 927-932, doi:10.1002/grl.50251, 2013.
- 657 Tanhua, T., and M. Liu: Upwelling velocity and ventilation in the Mauritanian upwelling system estimated by CFC-12 and SF₆
658 observations, *Journal of Marine Systems*, 151, 57-70, doi:10.1016/j.jmarsys.2015.07.002, 2015.
- 659 Thiele, G., and J. L. Sarmiento: Tracer Dating and Ocean Ventilation, *Journal of Geophysical Research-Oceans*, 95(C6), 9377-
660 9391, doi:10.1029/JC095iC06p09377, 1990.
- 661 Thomas, J. L., D. W. Waugh, and A. Gnanadesikan: Relationship between Age and Oxygen along Line W in the Northwest
662 Atlantic Ocean, *Ocean Science Journal*, 55(2), 203-217, doi:10.1007/s12601-020-0019-5, 2020.
- 663 Tomczak, M.: Some historical, theoretical and applied aspects of quantitative water mass analysis, *Journal of Marine Research*,
664 57(2), 275-303, doi:10.1357/002224099321618227, 1999.
- 665 Tseitlin, V.: Depth dependence of oxygen utilization rate, *OKEANOLOGIYA*, 32(2), 264-269, 1992.
- 666 van Heuven, S., M. Hoppema, O. Huhn, H. A. Slagter, and H. J. W. de Baar: Direct observation of increasing CO₂ in the
667 Weddell Gyre along the Prime Meridian during 1973-2008, *Deep-Sea Research Part II-Topical Studies in Oceanography*,
668 58(25-26), 2613-2635, doi:10.1016/j.dsr2.2011.08.007, 2011.
- 669 Wang, W. M., M. G. Cai, P. Huang, H. W. Ke, M. Liu, L. H. Liu, H. X. Deng, B. J. Luo, C. H. Wang, X. H. Zheng, W. Q. Li:
670 Transit Time Distributions and Apparent Oxygen Utilization Rates in Northern South China Sea Using Chlorofluorocarbons
671 and Sulfur Hexafluoride Data, *Journal of Geophysical Research-Oceans*, 126(8), doi:10.1029/2021jc017535, 2021.
- 672 Warner, M. J., and R. F. Weiss: Solubility of Chlorofluorocarbon-11 and Chlorofluorocarbon-12 in water and seawater, *Deep-*
673 *Sea Res*, 32(12), 1485-1497, doi:10.1016/0198-0149(85)90099-8, 1985.
- 674 Waugh, D. W., T. M. Hall, and T. W. N. Haine: Relationships among tracer ages, *Journal of Geophysical Research: Oceans*,
675 108(C5), doi:10.1029/2002jc001325, 2003.
- 676 Waugh, D. W., T. W. N. Haine, and T. M. Hall: Transport times and anthropogenic carbon in the subpolar North Atlantic Ocean,
677 *Deep Sea Research Part I: Oceanographic Research Papers*, 51(11), 1475-1491, doi:10.1016/s0967-0637(04)00145-1, 2004.
- 678 Ziska, F., B. Quack, K. Abrahamsson, S. D. Archer, E. Atlas, T. Bell, J. H. Butler, L. J. Carpenter, C. E. Jones, N. R. P. Harris,
679 H. Hepach, K. G. Heumann, C. Hughes, J. Kuss, K. Krüger, P. Liss, R. M. Moore, A. Orlikowska, S. Raimund, C. E. Reeves,
680 W. Reifenhäuser, A. D. Robinson, C. Schall, T. Tanhua, S. Tegtmeier, S. Turner, L. Wang, D. Wallace, J. Williams, H.
681 Yamamoto, S. Yvon-Lewis, and Y. Yokouchi: Global sea-to-air flux climatology for bromoform, dibromomethane and methyl
682 iodide, *Atmospheric Chemistry and Physics*, 13(17), 8915-8934, doi:10.5194/acp-13-8915-2013, 2013.

683
684